

Protein Kinase Inhibitor Design by Targeting the Asp-Phe-Gly (DFG) Motif: The Role of the DFG Motif in the Design of Epidermal Growth Factor Receptor Inhibitors

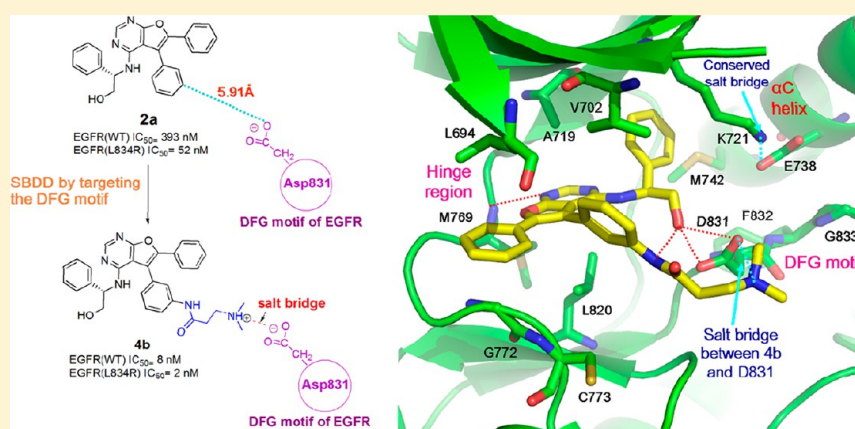
Yi-Hui Peng,[†] Hui-Yi Shiao,[†] Chih-Hsiang Tu,^{†,‡,||} Pang-Min Liu,^{†,||} John Tsu-An Hsu,[†] Prashanth Kumar Amancha,[†] Jian-Sung Wu,[†] Mohane Selvaraj Coumar,[§] Chun-Hwa Chen,[†] Sing-Yi Wang,[†] Wen-Hsing Lin,[†] Hsu-Yi Sun,[†] Yu-Sheng Chao,[†] Ping-Chiang Lyu,[‡] Hsing-Pang Hsieh,^{*,†} and Su-Ying Wu^{*,†}

[†]Institute of Biotechnology and Pharmaceutical Research, National Health Research Institutes, 35 Keyan Road, Zhunan Town, Miaoli County 350, Taiwan, ROC

[‡]Institute of Bioinformatics and Structural Biology, National Tsing Hua University, 101, Sect. 2, Guangfu Road, Hsinchu 300, Taiwan, ROC

[§]Centre for Bioinformatics, School of Life Sciences, Pondicherry University, Kalapet, Puducherry 605014, India

Supporting Information



ABSTRACT: The Asp-Phe-Gly (DFG) motif plays an important role in the regulation of kinase activity. Structure-based drug design was performed to design compounds able to interact with the DFG motif; epidermal growth factor receptor (EGFR) was selected as an example. Structural insights obtained from the EGFR/2a complex suggested that an extension from the meta-position on the phenyl group (ring-5) would improve interactions with the DFG motif. Indeed, introduction of an *N,N*-dimethylamino tail resulted in 4b, which showed almost 50-fold improvement in inhibition compared to 2a. Structural studies confirmed this *N,N*-dimethylamino tail moved toward the DFG motif to form a salt bridge with the side chain of Asp831. That the interactions with the DFG motif greatly contribute to the potency of 4b is strongly evidenced by synthesizing and testing compounds 2a, 3g, and 4f: when the charge interactions are absent, the inhibitory activity decreased significantly.

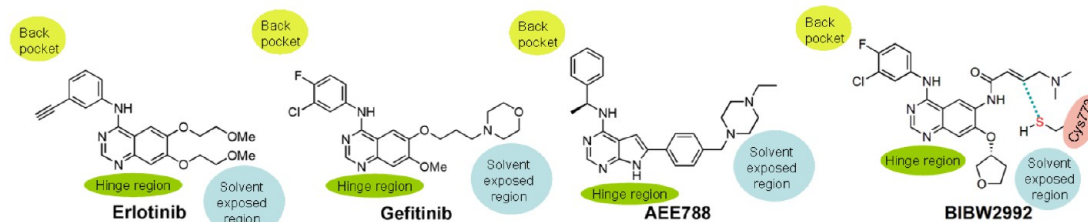
■ INTRODUCTION

The human genome encodes more than 500 protein kinases,¹ including tyrosine, serine/threonine, and dual specificity kinases. These kinases have a highly conserved catalytic domain, which binds the ATP molecule and magnesium ion at the site formed by the N- and C-terminal lobes.^{2,3} Regulatory elements within kinases serve to switch on and off the activity state of the protein.^{4,5} One such element is the activation loop, which regulates kinase activity through phosphorylation. Specifically, the activation loop undergoes large conformational changes, which switches the kinase between its inactive and active forms.⁴ When the activation loop is phosphorylated, it

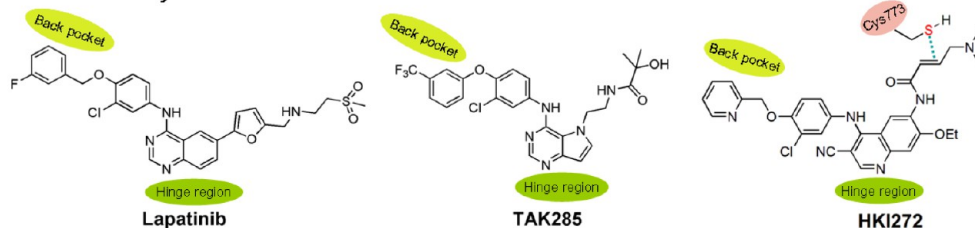
forms an open and extended conformation to allow substrate binding. The DFG motif located at the beginning of the activation loop is highly conserved among kinases and is important for protein catalysis.⁵ In active kinases, the DFG motif adopts an “in” conformation and the Asp residue is oriented toward bound ATP, which is able to coordinate the magnesium ion bound to the β - and γ -phosphate groups of ATP.⁶ In inactive kinases, the conformation of the DFG motif is flipped outward, such that the Asp no longer coordinates the

Received: January 15, 2013

I. Inhibitors bind to the hinge region and extend toward the solvent exposed region



II. Inhibitors expand to the ATP back pocket and disrupt the salt bridge between the helix α C and the conserved Lysine.



III. Inhibitor binds to the hinge region and interacts with the DFG motif

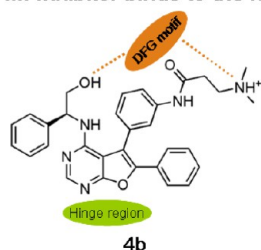


Figure 1. Structures of EGFR small molecule inhibitors and their bindings to EGFR.

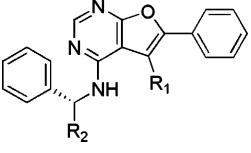
magnesium at the catalytic site.⁷ Another regulatory element is the position of the helix α C.⁵ In the active form of kinases, a salt bridge that coordinates the phosphate groups of ATP can be observed between the glutamate residue on helix α C and lysine residue on the N-lobe.⁸ In inactive kinases, the helix α C moves out of position and loses this salt bridge interaction. By the coordination of these regulatory elements, the protein kinases are able to phosphorylate substrate by transferring the γ -phosphate of ATP onto the side chain of protein substrate.

Protein kinases regulate many critical cellular processes through protein phosphorylation, such as proliferation and differentiation,⁹ and therefore constitute an important drug discovery opportunity.¹⁰ Among these kinases, the family of human ErbB receptor tyrosine kinase, also called epidermal growth factor receptor (EGFR), is an important drug target in oncology. The human EGFR family comprises four related members, HER-1(EGFR), HER-2, HER-3, and HER-4, which play central roles in cell proliferation and differentiation.⁹ Deregulation of the EGFR family pathway by overexpression or constitutive activation induces numerous cancers.¹⁰ Overexpression of EGFR family kinases is often observed in tumors, including colorectal, lung, breast, head, and neck carcinomas.¹¹ All proteins in the EGFR family are transmembrane proteins, containing an extracellular ligand binding domain, a transmembrane domain, an intracellular receptor tyrosine kinase domain, and a C-terminal signaling tail domain. The members of the EGFR family share high structural homology in their tyrosine kinase domain but are distinct in their extracellular and C-terminal domains.¹² The binding of growth factors to the extracellular domain induces receptor homo- or heterodimerization and activates the kinase domain, which would lead to the

autophosphorylation of the intracellular tyrosine residues at the C-terminal and the subsequent induction of downstream signals.^{13,14}

Various approaches have been developed to target the EGFR signaling pathway, including monoclonal antibodies and small molecule tyrosine kinase inhibitors (TKIs). Cetuximab,¹⁵ which has been approved by the FDA for the treatment of colorectal cancer, is a monoclonal antibody targeting the EGFR extracellular ligand-binding domain. TKIs targeting the intracellular kinase domain have also been developed with three such drugs having received FDA approval for use as cancer therapies: gefitinib,^{16,17} erlotinib,¹⁴ and lapatinib^{18,19} (Figure 1). Gefitinib and erlotinib are EGFR inhibitors used in the treatment of non-small cell lung cancer (NSCLC), while lapatinib, which inhibits EGFR and HER-2 kinases, is used in combination therapy for HER2-positive breast cancer. Clinical trials are currently evaluating the feasibility of additional drugs which target the EGFR pathway, including other reversible inhibitors [(6-(4-((4-ethylpiperazin-1-yl)methyl)phenyl)-N-((S)-1-phenylethyl)-7H-pyrrolo[2,3-d]pyrimidin-4-amine (AEE788),^{17,20} ((S)-morpholin-3-yl)methyl 4-(1-(3-fluorobenzyl)-1H-indazol-5-ylamino)-5-methylpyrrolo[1,2-f][1,2,4]-triazin-6-ylcarbamate (BMS-599626),²¹ and N-(2-(4-(4-(3-(trifluoromethyl)phenoxy)-3-chlorophenylamino)-5H-pyrrolo[3,2-d]pyrimidin-5-yl)ethyl)-2-hydroxy-2-methylpropanamide (TAK-285)^{22,23}] as well as irreversible inhibitors [(E)-N-(4-(4-(pyridin-2-yl)methoxy)-3-chlorophenylamino)-3-cyano-7-ethoxyquinolin-6-yl)-4-(dimethylamino)but-2-enamide (HKI-272),^{24,25} N-(3-(2-(2-methoxy-4-(4-methylpiperazin-1-yl)-phenylamino)-5-chloropyrimidin-4-ylamino)phenyl)acrylamide (WZ4002),²⁶ (E)-N-(7-((R)-tetrahydrofuran-3-yloxy)-4-(3-

Table 1. EGFR Inhibition of Furanopyrimidine Analogues



Compound	R ₁	R ₂	EGFR inhibition, ^a IC ₅₀ (nM)	
			WT	L834R
2a	Ph	CH ₂ OH	393	52
2b	Ph	Me	2,991	339
2c	Ph	Et	> 10,000	> 10,000
2d	Ph	CO ₂ Me	7,893	1,451
2e	Cl	CH ₂ OH	589	168
2f	Br	CH ₂ OH	452	90
3a	2-Furan	CH ₂ OH	434	73
3b	3-Furan	CH ₂ OH	352	44
3c	3-OCH ₂ O-4-Ph	CH ₂ OH	258	30
3d	3-NO ₂ -Ph	CH ₂ OH	820	49
3e	3-NH ₂ -Ph	CH ₂ OH	203	22
3f	4-NHAc-Ph	CH ₂ OH	179	23
3g	3-NHAc-Ph	CH ₂ OH	218	29
Gefitinib	--	--	33	15

^aValues are expressed as the mean of at least three independent determinations and are within $\pm 15\%$

chloro-4-fluorophenylamino)quinazolin-6-yl)-4-(dimethylamino)but-2-enamide (BIBW2992),^{27,28} and (*E*)-*N*-(4-(3-chloro-4-fluorophenylamino)-7-methoxyquinazolin-6-yl)-4-(piperidin-1-yl)but-2-enamide (PF-00299804)^{29,30}].

Nonetheless, EGFR inhibitors have been shown to cause a variety of adverse effects in patients. For example, interstitial lung disease (ILD) is a common, serious adverse effect experienced by patients with advanced NSCLC after receiving gefitinib treatment.^{31,32} In 2009, the U.S. FDA warned that the use of erlotinib could result in serious disorders in the gastrointestinal tract, skin, and eyes. Lapatinib has been associated with hepatotoxicity when used in combination with other chemotherapies.³³ Even the second-generation irreversible inhibitor BIBW2992 produced adverse effects: diarrhea (95%) and rash (62%) were observed in clinical trials³⁴ although rash has also been regarded as a positive sign of efficacy. The side effects associated with these EGFR inhibitors may be related to the cross activity with other kinases. For example, in addition to inhibiting EGFR, erlotinib also exhibited strong inhibition effects against serine/threonine kinase 10 (STK10). The inhibition of STK10 has been found to increase lymphocytic responses, such as cell migration and interleukin-2 secretion, and consequently to result in severe skin disorders.³⁵

Many EGFR inhibitors contain a quinazoline core scaffold, including reversible inhibitors, such as erlotinib, gefitinib, and lapatinib, and the irreversible inhibitors BIBW2992, (*E*)-*N*-(4-(3-chloro-4-fluorophenylamino)-3-cyano-7-ethoxyquinolin-6-yl)-4-(dimethylamino)but-2-enamide (EKB-569),³⁶ and HKI-272. A few diverse core scaffolds can be found in recent studies, such as TAK-285 (derived from a pyrrolo[3,2-*d*]pyrimidine scaffold²²), which is a dual EGFR/HER2 inhibitor under clinical development. All of these inhibitors share a common

feature: upon the binding to EGFR, a hydrogen bond forms between the N1 atom of the quinazoline or pyrimidine core and the backbone NH of Met769 in the hinge region.^{14,25,37}

Analysis of previously published structures (PDB codes: 1M17,¹⁴ 2ITY,¹⁷ 2J6M,¹⁷ 3POZ,²³ 2JIV,²⁵ 4GSJ,²⁸ and 1XKK³⁷) of small molecule inhibitors binding to EGFR revealed two binding modes (Figure 1). The first mode is characterized by the core structure of inhibitors forming strong interactions with the hinge region in EGFR and the other moiety of inhibitors extending to (or close to) the solvent exposure area. The inhibitors also expand to the ATP back pocket. Examples of inhibitors adopting this binding mode are erlotinib, gefitinib, AEE788, and BIBW2992 (Figure 1). In the second mode, the core structure of inhibitors, such as lapatinib, TAK-285, and HKI272 (Figure 1), forms H-bond and hydrophobic interactions with the hinge region while the lipophilic moiety of the inhibitors expands to the back pocket of the ATP binding site and disrupts the salt bridge between the glutamate residue on helix α C and the lysine residue on the N-lobe.

In this study, we designed the EGFR inhibitors specifically targeting the DFG motif because of the important role played by the DFG motif in the regulation of kinase activity. We selected a furanopyrimidine scaffold hit compound, **2a**, which had been discovered in our previous research via high-throughput screening,³⁸ and then employed a structure-based drug design approach to develop compounds able to interact with the DFG motif. Through the structure-guided design, a novel compound, **4b**, was identified and found to have almost 50-fold improvement in EGFR inhibition as compared to the hit compound **2a**. Compound **4b** displayed an EGFR inhibition better than that of gefitinib. Further structural biology studies confirmed that **4b** interacts with the DFG motif through the

N,N-dimethylamino tail to form a salt bridge with the side chain of Asp831.

RESULTS AND DISCUSSION

Chemistry. Approximately 20 furanopyrimidine derivatives (Tables 1 and 2) were synthesized as shown in Scheme 1.

Table 2. EGFR Inhibition of Furanopyrimidine Analogues

Compound	R	EGFR inhibition, ^a IC ₅₀ (nM)	
		WT	L834R
3g		218	29
4a		48	4
4b		8	2
4c		29	34
4d		34	4
4e		4,327	486
4f		> 25,000	1,270
AEE788	--	40	9
Gefitinib	--	33	15

^aValues are expressed as the mean of at least three independent determinations and are within $\pm 15\%$

Starting materials **1a–c** were prepared³⁸ and reacted with various chiral amines via an S_NAr reaction to give chiral compounds **2a–f**. Suzuki coupling reactions were then employed to couple bromo compound **2f** with various substituted aryl boronic acids, yielding coupling products **3a–g**. Finally, reacting **3e** with the corresponding carboxylic acid in the presence of EDC yielded the desired compounds **4a–f**. All compounds were characterized by ¹H NMR and LC-MS, and their purity was determined by reverse phase HPLC.

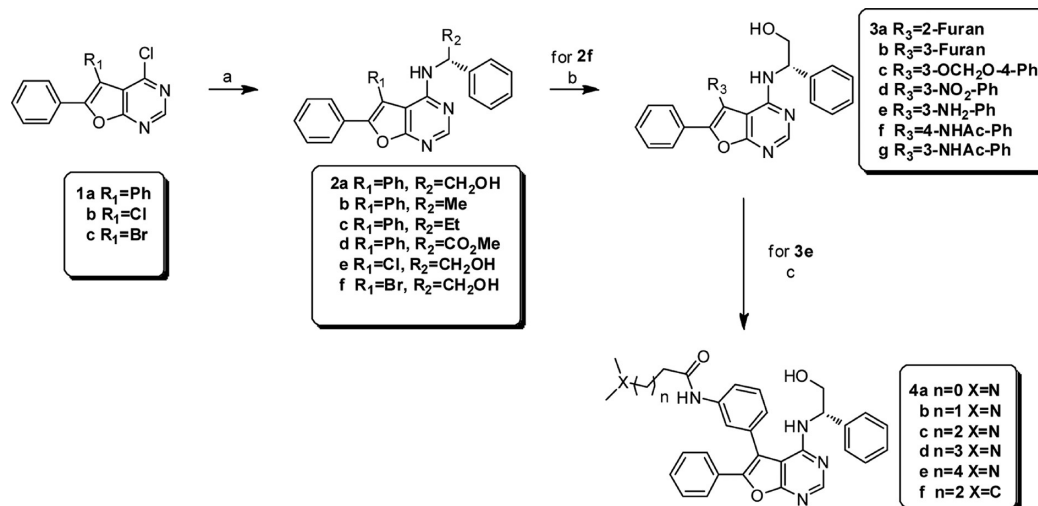
SAR Studies. Compound **2a**,³⁸ previously discovered by us, was used as starting point for a structure–activity and lead optimization study.

A variety of substituted derivatives (**2a–3e**; Table 1) were synthesized and evaluated by biological assays. In addition to wild-type EGFR, the synthesized compounds were also screened for their inhibition against the L834R mutant (also identified as L858R in an alternative numbering of the human EGFR sequence), which has been reported³⁹ to be present in NSCLC patients.

2a inhibited wild-type EGFR and L834R mutant, with IC₅₀ values of 393 and 52 nM, respectively. Replacement of the primary hydroxyl group of **2a** with various alkyl groups to produce **2b** (methyl group), **2c** (ethyl group), or **2d** (ester group) resulted in a dramatic decrease in inhibitory activity against both wild-type and L834R mutant EGFR. This suggests that the primary hydroxyl group at the R₂ substitution position contributes greatly to the EGFR inhibition.

Next, the role of the R₁ substituent at the third position of the furanopyrimidine core was investigated. Introducing an electron-withdrawing halogen, such as chlorine **2e** or bromine **2f**, at this position resulted in slightly lower inhibition compared with the phenyl substitution of **2a**. On the other hand, introduction of furan derivatives to give **3a** and **3b** resulted in retention of activity, and when the phenyl ring was replaced with a 1,3-benzodioxole moiety to give **3c**, activity slightly improved. Moreover, of the substituted phenyl derivatives **3d–e**, the amine-bearing substituent **3e** showed improved inhibitory activity compared with **2a**. In contrast, introduction of a nitro group in substituent **3d** decreased activity. As **3e** not only exhibited strong inhibition against EGFR but also possessed an extensible amino group, it was selected for further lead optimization.

Structural Biology Study of Compound 2a. Concurrently with the aforementioned SAR study, **2a** was cocrystallized with the wild-type EGFR kinase domain and the structure complex was solved in order to elucidate the binding mode and obtain the structural insights necessary to design a more potent EGFR kinase inhibitor. The electron density maps of EGFR in complex with **2a** clearly shows that EGFR adopts an active conformation with a salt bridge between Lys721 and Glu738, and **2a** is located in the ATP binding cleft between the N- and C-lobes (Figure 2B). The furanopyrimidine core (ring-2 and ring-3) of **2a** (Figure 2A,B) aligns in the hinge region of EGFR, forming one H-bond with the main chain of Met769 and making hydrophobic interactions with surrounding residues, including Leu694, Ala719, Met769, and Leu820 (Figure 2A,B). The phenyl moiety (ring-1) (Figure 2A) also forms extensive hydrophobic interactions with residues of Val702, Ala719, Lys721, Leu764, and Thr766 in the N-lobe β -sheet and Met742 in the α C helix. The phenyl moiety (ring-4) at the second position on the furan moiety makes close contact with Leu694 and Gly772. (Figure 2A,B). The phenyl substitution (ring-5) at the R₁ position is perpendicular to the furanopyrimidine core (Figure 2A,B). It forms hydrophobic interactions with Leu694 on the glycine-rich loop (P-loop) and Val702 in the N-lobe β -sheet. Interestingly, the primary hydroxyl group of **2a** forms an H-bond with the side chain of Asp831 on the DFG motif (Asp831-Phe832-Gly833 in EGFR). The importance of the H-bond interaction between this primary hydroxyl group and the carboxylate group of Asp831 is revealed in a SAR study (Table 1), which shows that when this primary hydroxyl group is replaced with alkanes, such as a methyl group **2b** and **2d** or a ethyl group **2c**, the H-bond interaction is lost and inhibitory activity is greatly reduced. Because a polar hydroxyl group at R₂ substitution site has

Scheme 1. Construction of Furanopyrimidine Compounds^a

^aReagents and conditions: (a) amine, EtOH, Et₃N, reflux; (b) boronic acid, Pd(dppf)Cl₂, Na₂CO₃, dioxane, reflux; (c) carboxylic acid, EDCl, DCM, rt.

proved to be a potent functional group to retain the activity, it is therefore maintained in the further lead optimization.

Structure-Based Drug Design of Furanopyrimidine Compounds. The DFG motif regulates the catalysis of protein kinase and contributes to ATP binding.⁵ The important biological function of DFG suggested to us that modification of the hit compound by targeting the DFG motif would enhance the activity. Indeed, the EGFR/2a structure (Figure 2B) showed that the distances from meta- and para-positions on the perpendicular phenyl group (ring 5) to the side chain of Asp831 are 5–7 Å (meta distance to the OD2 atom of Asp831 is 5.91 Å, and para distance to the OD2 atom of Asp831 is 6.80 Å), which allowed the extension of an appropriate moiety to interact with the DFG motif. Following this rational design approach, 3g and 3f bearing an acetamide moiety at the meta and para positions, respectively, were synthesized. Both compounds displayed slightly increased inhibition of EGFR kinase compared with 2a (Table 1). The following structural biology study of 3g (Figure 2B) in complex with EGFR confirmed that the amide substituted moiety moved toward the DFG motif as expected with a shorter distance to Asp831 (distance between the C24 atom in 3g and the OD2 atom of Aps831 is 3.76 Å).

To enhance the interactions of 3g with the DFG motif, a series of meta-substituents bearing a *N,N*-dimethylamino group attached to different lengths of carbon chain were synthesized (Table 2). It was thought that the cationic amino group could form a strong ionic interaction with the deprotonated carboxylic acid side chain of Asp831. Indeed, the activity of amine-bearing 3g derivatives (4a–d) toward both wild-type EGFR and L834R mutant was improved. Compound 4b, containing a two carbon-chain linker, was the most potent compound, with a 49-fold improvement in wild-type activity and 26-fold improvement in L834R activity compared with 2a. It also showed improved activity compared with gefitinib (4-fold and 7-fold improvement in wild-type and L834R mutant, respectively). However, when the length of the alkyl chain was increased to five carbons (4e), a dramatic loss of activity was observed, particularly in wild-type EGFR. Thus, this SAR study suggested the appropriate chain length of compound would

provide a suitable conformation to bind and inhibit EGFR activity.

When the nitrogen atom of the terminal *N,N*-dimethylamino group of 4c was replaced with a carbon atom to generate 4f (Table 2), a nearly complete loss of activity ($\text{IC}_{50} > 25 \text{ uM}$) resulted, indicating that the *N,N*-dimethylamino group plays an important role in the inhibition of EGFR.

Binding Mode of 4b in EGFR. Because the introduction of the ethyl *N,N*-dimethylamino moiety to compound 3g greatly improved the inhibitory activity in EGFR, the crystal structure of 4b in complex with EGFR was solved in order to rationalize the observed structure–activity relationship trend. The structure was determined at 2.83 Å resolution (Supporting Information Table S1) and showed a clear electron density map. Compound 4b binds to the active form of EGFR, which is characterized by a salt bridge between Lys721 and Glu738 (Figure 3A). The structure of EGFR/4b presents a very special and strong hydrogen bond network in the ATP binding pocket (Figure 3A). First, the N-6 nitrogen atom on the core pyrimidine ring (ring-2) (Figure 2A) forms a conserved hydrogen bond with Met769 in the hinge region (Figure 3A). Second, the primary hydroxyl group at the R₂ position forms very strong H-bonds with the side chain of Asp831 in the DFG motif. And last, but most significantly, the cationic dimethylamino group forms a salt bridge with the anionic carboxylate group of Asp831 in the DFG motif (Figure 3A). This structure revealed that 4b acted like a “clamp” that wrapped around Asp831 to block ATP binding and therefore prevent phosphate transfer to downstream protein of the signal transduction pathway. Without the *N,N*-dimethylaminoethyl moiety (2a and 3g), the salt bridge interaction was lost and the inhibition activity greatly decreased. In particular, the nitrogen atom in the *N,N*-dimethylamino group serves as a base to interact with the acidic side chain of Asp831. The importance of this electrostatic interaction is emphasized by the fact that compound 4f, in which the positively charged nitrogen atom was replaced with a neutral carbon atom, is a very poor inhibitor.

In addition to H-bond and charge interactions, 4b also forms strong hydrophobic interactions at the ATP binding site

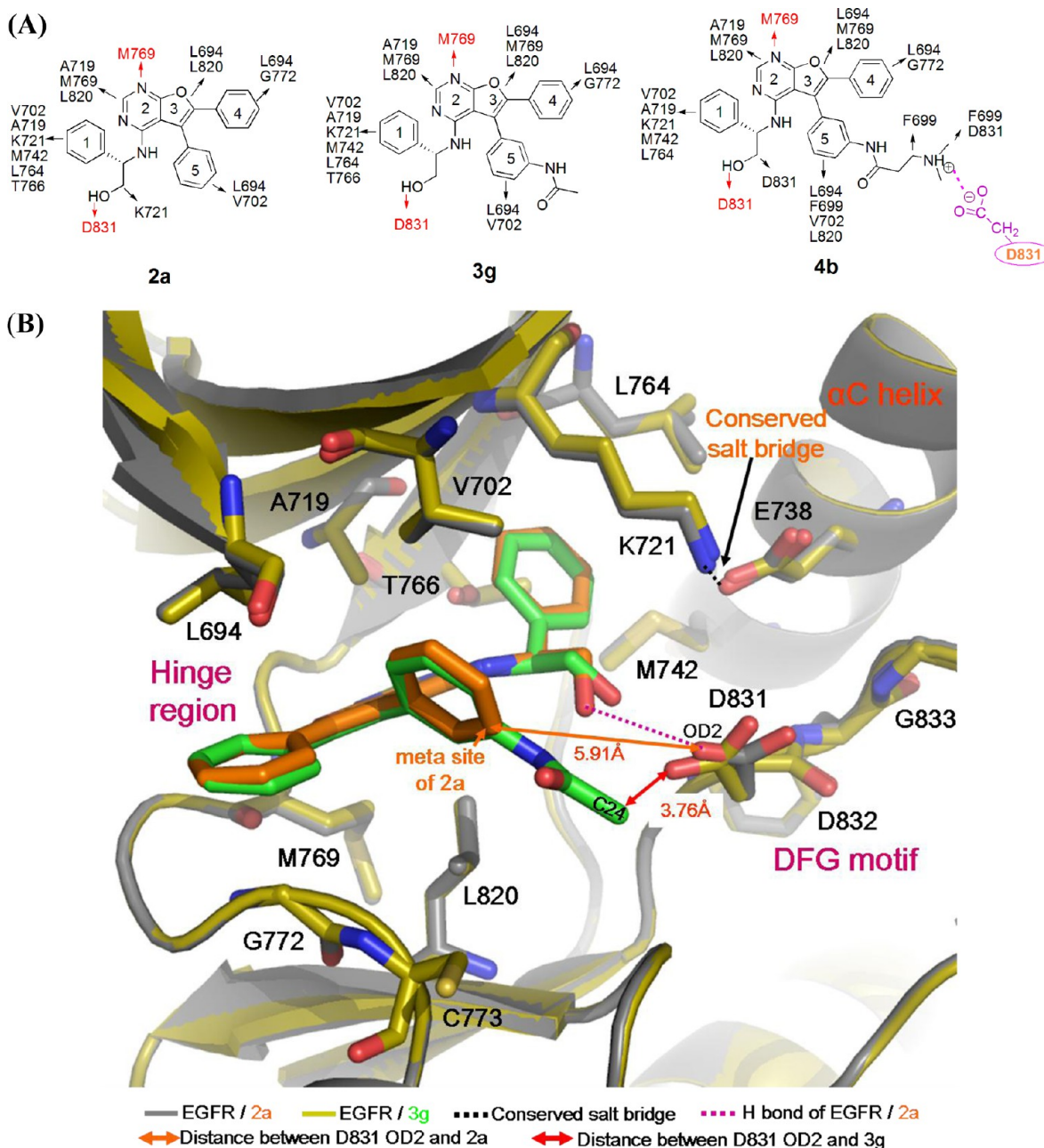


Figure 2. (A) Interactions of 2a, 3g, and 4b with EGFR. Hydrogen bonds are shown in red. Hydrophobic interactions are shown in black. Salt bridges are shown in pink. (B) Superimposition of structures of compound 2a (orange) and 3g (green) with EGFR. The distance of the meta position on ring-5 of 2a to the carboxyl group (OD2 atom) of Asp831 is 5.91 Å (orange line), while adding the acetamide group to this meta position, the shortest distance between 3g (C24 atom) with the carboxyl group (OD2 atom) of Asp831 decreases to 3.76 Å (red line). The H-bond between the primary hydroxyl group of 2a and Asp831 is shown with a magenta dotted line. For clarity, the H-bond between 2a and the residue M769 and all H-bonds between 3g and EGFR are omitted.

(Figures 2A and 3A). The ring-1 forms hydrophobic interactions with Val702, Ala719, Lys721, Met742, and Leu764 located in the N lobe of the EGFR kinase domain. The furanopyrimidine core (ring-2 and ring-3) aligns in the hinge region and forms hydrophobic interactions with Leu694, Ala719, Met769, and Leu820. The ring-4, located near the solvent exposed region, makes close contact with Leu694 and Gly772. The perpendicular ring-5 forms hydrophobic interactions with Leu694, Phe699, Val702, and Leu820.

Comparison of the Structure of EGFR/4b with the Structure of EGFR/2a. The structure of the EGFR/4b complex was compared with the structure of the EGFR/2a

complex to understand the enhanced potency of 4b and examine the differences in interactions at the molecular level (Figure 3B). A detailed comparison of the binding features of these two inhibitors is summarized in Table 3. The two compounds adopt very similar conformations, and their aromatic rings superimpose well. The most significant difference between these inhibitors is an additional tail of 4b, which provides additional salt bridge interactions with the protein. Moreover, in comparison with structure of EGFR/2a, the side chain of Asp831 rotates and moves closer to the primary hydroxyl group, resulting in the formation of an additional H-bond between 4b and the DFG motif. An extra intramolecular

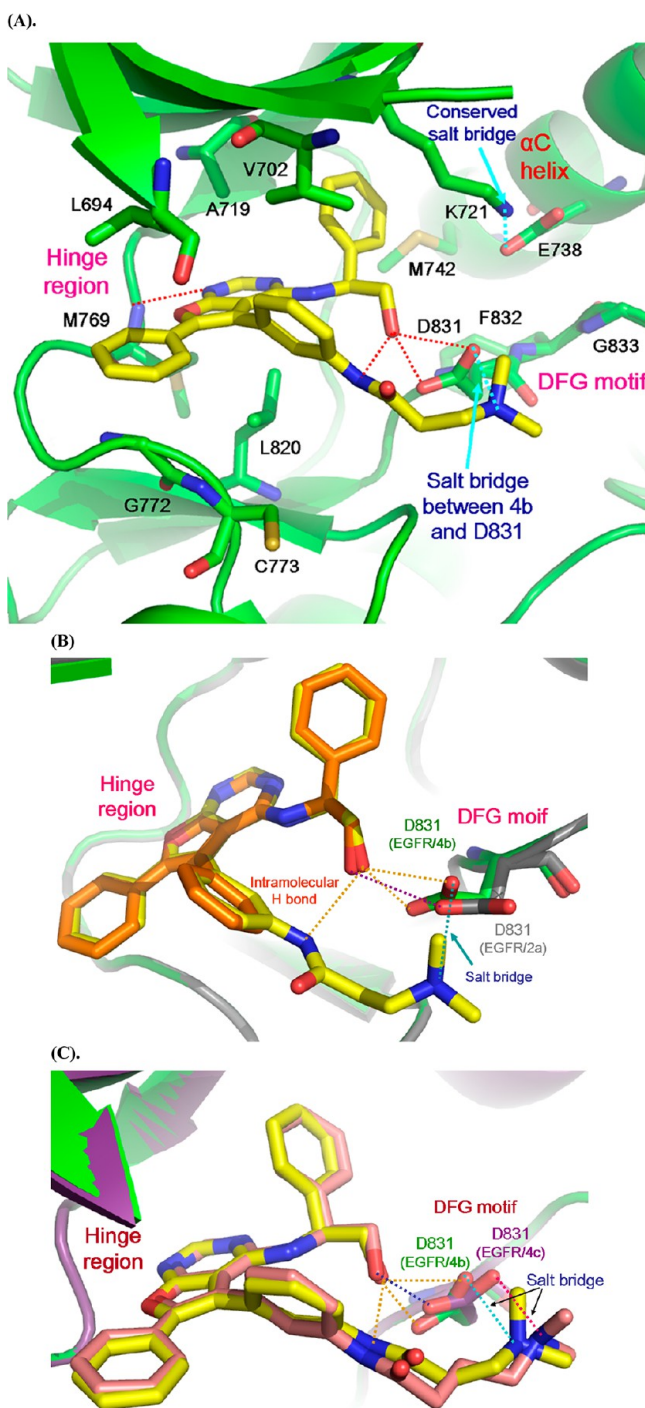


Figure 3. (A) Structure of furanopyrimidine compound **4b** (yellow) bound to EGFR. (B) Superimposition of structures of EGFR (gray)/**2a** (orange) with EGFR (dark-green)/**4b** (yellow). The intramolecular and intermolecular H-bonds between **4b** and Asp831 are shown with brown dotted lines; the H-bond between **2a** and Asp831 is depicted with a purple dotted line; the salt bridge between **4b** and Asp831 is shown with a light-blue dotted line. (C) Superimposition of structures of EGFR (dark-green)/**4b** (yellow) with EGFR (purple)/**4c** (light-orange). The H-bond between **4c** and Asp831 is depicted with a dark-blue dotted line; the salt bridge between **4c** and Asp831 is shown with a magenta dotted line.

H-bond is also observed between the oxygen atom on the hydroxyl group (H-bond acceptor) and amine group (H-bond donor) attached to ring-5 in **4b**, whereas this intramolecular H-

Table 3. The Summary of Interactions between Inhibitors and EGFR

Compound	2a	3g	4b	4c
Structure				
EGFR Inhibition Activity (IC ₅₀) (nM)	393	218	8	29
EGFR ^{L834R} Inhibition Activity (IC ₅₀) (nM)	52	29	2	34
H-bond with the hinge (M769)	Yes	Yes	Yes	Yes
H-bond with the DFG motif (D831)	Yes	Yes	Yes	Yes
Salt bridge with the DFG motif (D831)	No	No	Yes	Yes
Intramolecular H-bond	No	No	Yes	No
Distance to D831 (Å)	5.91 (Meta site to the OD2 atom of D831)	3.76 (C24 atom to the OD2 atom of D831)	< 4.00 (Form the salt bridge interaction)	< 4.00 (Form the salt bridge interaction)

bond is absent in **2a**. We hypothesize that the *N,N*-dimethylamino tail of **4b**, through the interactions with Asp831, brings the nitrogen atom close to the hydroxyl group and consequently leads to the formation of the strong intramolecular H-bond. This intramolecular H-bond might stabilize the structure of the compound and therefore contributes to the improved activity of **4b**.

In summary, an additional hydrogen bond, strong salt bridge interactions, and extra intramolecular H-bond interactions could explain the enhanced activity of **4b**.

The Effects of Various Tail Lengths. As revealed in the SAR study (Table 2), tails of various length differ in their effects on the inhibition of EGFR and the two carbon chain length of *N,N*-dimethylamino tail (**4b**) has the optimal activity. To investigate the differences at the molecular level, the crystal structure of EGFR/**4c** was solved and compared with that of EGFR/**4b** (Figure 3C, Table 3). Although two structures adopt very similar conformations, some differences were observed, particularly in the *N,N*-dimethylamino tail, the primary hydroxyl group, and Asp831 (Figure 3C). The *N,N*-dimethylamino tail of **4c** (with one extra carbon in the chain) extends further toward the activation loop, and the side chain of Asp831 in the EGFR/**4c** structure consequently shifts to maintain the salt bridge interactions with the *N,N*-dimethylamino tail. Interestingly, the movement of Asp831 in the EGFR/**4c** structure toward the *N,N*-dimethylamino tail concurrently shifts Asp831 away from the primary hydroxyl group and consequently leads to the loss of one H-bond interaction with the primary hydroxyl group. This might explain the weaker inhibition of **4c** as compared with **4b**. When the chain length increased to five carbons (**4e**), the activity decreased by 540-fold. The reason for this dramatic loss of activity could be that the *N,N*-dimethylamino group would be far away from the DFG motif and so could not form the salt

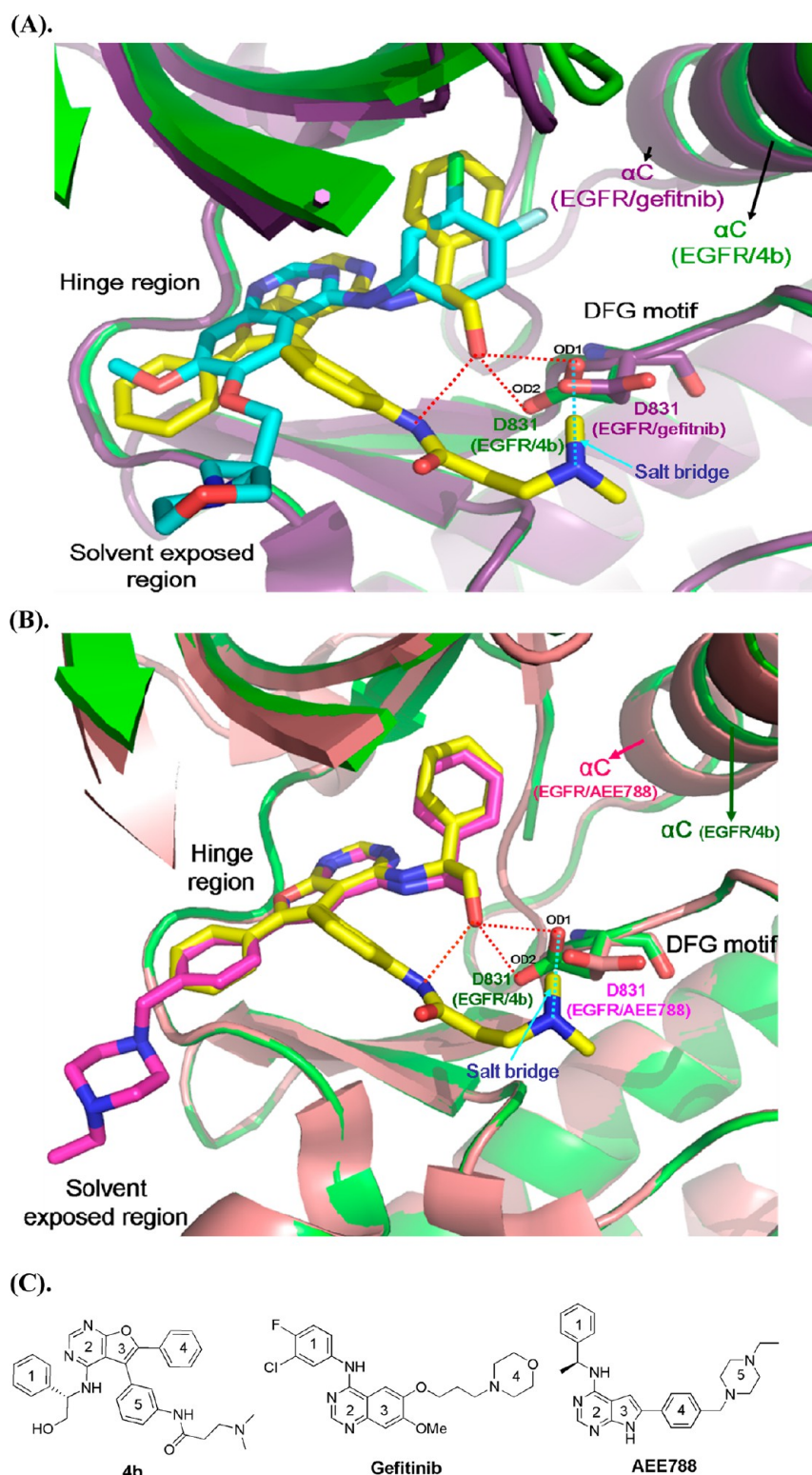


Figure 4. (A) Comparison of structures of EGFR (green)/4b (yellow) and EGFR (purple)/gefitinib (cyan). (B) Comparison of structures of EGFR (green)/4b (yellow) and EGFR (pink)/AEE788 (magenta). (C) Structures of 4b, gefitinib, and AEE788. For comparison, the rings of compound structures are labeled.

bridge interactions with the side chain of Asp831. Another possibility is that the flexible side chain of Asp831 could move closer to the *N,N*-dimethylamino group to interact with the tail, resulting in the loss of important H-bonds with the primary hydroxyl group.

The interactions between the primary hydroxyl and the *N,N*-dimethylamino group of compounds with the DFG motif of EGFR are two main factors that determine the potency of the inhibitors. 4b, with a two carbon-chain tail, adopts the best conformation to allow the optimal interactions of the primary hydroxyl and *N,N*-dimethylamino group with the DFG motif.

Comparison with the Structures of Other Inhibitors

Bound to EGFR. First, the X-ray cocrystal structures of **4b** and gefitinib (Figure 4A) were compared. Overlapping the structures of these two complexes revealed that the furanopyrimidin moiety (ring-2 and ring-3) of **4b** superimposes well with the quinazoline core (ring-2 and ring-3) of gefitinib (Figure 4C) to form the conserved H-bonds with Met769. The ring-1 of **4b** and the 3-chloro-4-fluoro-aniline (ring-1) of gefitinib both extend to the hydrophobic pocket in the back of the ATP-binding cleft and point toward the C-helix; however, the ring-1 of **4b** makes more extensive hydrophobic interactions with the surrounding residues. The ring-4 of **4b** occupies a similar position with the methoxy group of gefitinib, which is aligned with the hinge connection loop. The significant difference occurs in the ring-5 bearing *N,N*-dimethylamino tail of **4b**, which adopts a spatial position different from the propyl morpholino moiety of gefitinib. The tail part of **4b** directs toward the DFG motif and forms a salt bridge with Asp831, while the propyl morpholino group of gefitinib extends to the solvent exposed region. Moreover, the carboxylic side chain of Asp831 induces conformational changes to form strong electrostatic interactions with the tail of **4b** and allow the formation of H-bonds with the primary hydroxyl; in contrast, the carboxylic side chain of Asp831 of the EGFR/gefitinib structure adopts a conformation similar to the apo EGFR and has no interactions with gefitinib.

The structure of EGFR/**4b** was also compared with that of EGFR/AEE788 (Figure 4B). By superimposing the structure complex of AEE788 onto **4b**, it was found that rings 1–4 of AEE788 superimpose well with rings 1–4 of **4b** (Figure 4C). The major difference was the orientation of the piperazine moiety of AEE788, which adopts a spatial position different from that of the ring-5 of **4b** (the ring bearing the *N,N*-dimethylamino tail). The piperazine moiety of AEE788 occupies the solvent exposed region and does not interact with any protein residues of EGFR. In contrast, the *N,N*-dimethylamino tail of **4b** greatly contributes to the improved activity through interactions with the DFG motif. Moreover, the H-bond interaction with Asp831 is lost in the structure of EGFR/AEE788 because of the absence of a substituted hydroxyl group. The additional salt bridge interactions and the H-bond with the DFG motif may explain the better inhibition of **4b** compared with AEE788 (Table 2).

Kinase Profiling. Because of the high degree of homology of the ATP binding site among all kinases, a small molecular inhibitor may inhibit many protein targets simultaneously. To assess the selectivity of **4b** over other kinases, we profiled **4b** over a panel of 317 kinases, including EGFR and HER2 (Supporting Information Table S2). The assay to test the ability of **4b** to inhibit these kinases was performed at 1 μ M concentration. The results showed that **4b** indeed inhibits EGFR, wild-type (99% at 1 μ M), L834R mutant (100% at 1 μ M), and L837Q mutant (106% at 1 μ M), better than all of the other tested kinases. Of the 317 kinases profiled, only eight kinases (eight of 317, or 2%) including three EGFR proteins (wild-type, L834R, and L837Q mutants) were strongly inhibited by **4b** (>80% inhibition at 1 μ M concentration). Compound **4b** also showed between 50% and 80% inhibition against 14 other kinases, including two EGFR mutants (T766 M mutant and T766M/L834R double mutant).

CONCLUSION

In this study, a novel furanopyrimidine-based series of EGFR inhibitors was synthesized and structure-guided lead optimization by targeting the DFG motif of EGFR led to the identification of a potent EGFR inhibitor, **4b**. Structural insights obtained from X-ray cocrystal studies of **2a**, the initial compound discovered by our previous study, suggested that an extension from the meta-position on the perpendicular phenyl group (ring-5) would allow further interactions with the DFG motif and consequently improve inhibitor potency. Modification of meta-substituents with the *N,N*-dimethylamino group attached to carbon chains of different lengths improved the inhibition of **4b** by nearly 50-fold over that of **2a**. In addition, the potency of **4b** is superior to that of the commercial drug, gefitinib. The structure of EGFR in complex with **4b** revealed that the ethyl *N,N*-dimethylamino tail moves toward the DFG motif to form a salt bridge with the side chain of Asp831. That the interactions of this *N,N*-dimethylamino tail with the carboxylate group of Asp831 contribute greatly to the potency of **4b** is strongly evidenced by synthesizing and testing compounds **2a**, **3g**, and **4f**: the inhibitory activity of these compounds decreases significantly in the absence of charge interactions with the DFG motif.

The interactions of inhibitors with the DFG motif of protein kinases have been observed in a number of structures (PDB codes: 1IEP,⁴⁰ 3UP7,⁴¹ 3NPC,⁴² 1KV2,⁴³ 1KV1,⁴³ 4EYJ,⁴⁴ 3G6G,⁴⁵ 3G6H,⁴⁵ 2OIQ,⁴⁶ 2O08,⁴⁷ 2P4I,⁴⁸ 4F9B,⁴⁹ 4EOI,⁵⁰ 4BCI,⁵¹ 4GK2,⁵² 4ALW,⁵³ 3R7Q,⁵⁴ 3ZDI,⁵⁵ 4H1J,⁵⁶ 4BBF,⁵⁷ 4G9R,⁵⁸ 4HCU,⁵⁹ 4EQU,⁶⁰ and 2OJJ⁶¹). For example, the structure of p38 MAPK kinase bound to a diaryl urea inhibitor (PDB code: 1KV1) shows that the carbonyl group of the inhibitor forms a hydrogen bond with the backbone NH of Asp168 in the DFG motif. Another example is that the phenol moiety of the xanthine derivative inhibitor makes an H-bond interaction with the backbone NH of Asp764 in the DFG motif of erythropoietin-producing human hepatocellular carcinoma receptor A3 (EPHA3) tyrosine kinase (PDB code: 4GK2). H-bonds have also been observed between inhibitors and the side chain of Asp in the DFG motif in some structures. For example, in the structure of cell division cycle 7-related protein kinase (CDC7)/DBF4 protein kinase in complex with the inhibitor, the NH group in the pyridinone moiety of the inhibitor H-bonded with the side chain of Asp196 in the DFG motif (PDB code: 4F9B). Hydrophobic interactions and π - π interactions have been observed between inhibitors and DFG motifs as well. For example, in the crystal structure of B-Raf^{V600E} kinase in complex with the inhibitor (PDB code: 4G9R), the methylquinazoline moiety of the inhibitor makes π - π interactions with the side chain of Phe594 in the DFG motif. In another example, the structure of c-Src kinase in complex with a pyrimidine-based inhibitor (PDB code: 3G6H) revealed that the pyridine moiety of the inhibitor forms hydrophobic and π - π interactions with the side chain of Phe405 in the DFG motif. Most inhibitors form the H-bond, hydrophobic interactions, or π - π interactions with the DFG motif of kinases; however, charge interactions formed between the inhibitors and the DFG motif have rarely been observed. Our study demonstrates that the potency of EGFR inhibitors can be improved by targeting the DFG motif. Because the DFG motif plays an important role in the regulation of kinase activity and is highly conserved in almost all protein kinases, our strategy of designing inhibitors specifically to interact with the DFG motif

is an effective approach to improve the potency of compounds, both in the initial discovery as well as in the lead optimization phase.

Finally, it is worth noting that although compound **4b** was designed to target the highly conserved DFG motif, it exhibited high selectivity showing strong inhibition in a relatively small fraction of protein kinases (Supporting Information Table S2). The reasons this selectivity could be achieved with compound **4b** could be that the DFG motif adopts various conformations in different kinases. As discussed in the previous section, the proper spatial arrangement of **4b** with the DFG motif of EGFR is critical to the activity of the inhibitor. In the structures of other kinases, the conformation of the DFG motif is distinct from that of EGFR; therefore, the spatial arrangement of compound **4b** with other kinases will be different from that of EGFR. For example, the structural alignment of the EGFR/**4b** structure with Janus kinase 1 (JAK1)⁶² (PDB code: 3EYG) (Supporting Information Figure S1A) revealed that the DFG motif of JAK1 is located far from the *N,N*-dimethylamino group of **4b** and could not form charge interactions with the side chain of Asp1021. This would explain, at least partially, the very weak inhibition of compound **4b** on JAK1 (−14% inhibition at 1 μ M of **4b**). Another reason that compound **4b** showed selectivity even though it was designed to target the conserved motif could be that other residues within the ATP binding site also affect the binding of the inhibitor, such as the gatekeeper residue. It has been reported that the gatekeeper residue contributes to the selectivity of kinase inhibitors.⁶³ In the protein structure of cyclin-dependent kinase 2 (CDK2) kinase⁶⁴ (PDB code: 1FIN), the gatekeeper residue has a bulky side chain (Phe80) while, in EGFR, the gatekeeper residue has a small side chain (Thr766). Structural alignment of these two structures (Supporting Information Figure S1B) revealed that the side chain of Phe80 of CDK2 would cause a steric clash with the ring-1 of **4b**, which could be the reason for the loss of the inhibitory effect of **4b** on CDK2 (−4% inhibition at 1 μ M of **4b**). Therefore, if applying the strategy presented in this study to design kinase inhibitors, one should carefully analyze the structures of interest (structures with bound inhibitors are preferable) and take into account the conformation of the DFG motif together with other important structure features, such as the gatekeeper residue, the hinge loop, and the P-loop, to ensure the optimal fit of the designed inhibitor into the binding site.

■ EXPERIMENTAL SECTION

General Methods. All commercial chemicals and solvents are reagent grade and used as supplied unless otherwise noted. All reactions were carried out under an atmosphere of dry nitrogen. Reactions were monitored by TLC using Merck 60 F₂₅₄ silica gel glass backed plates (5 cm × 10 cm); zones were detected visually under ultraviolet irradiation (254 nm) or by spraying with phosphomolybdic acid reagent (Aldrich) followed by heating at 80 °C. Flash column chromatography was performed using silica gel (Merck Kieselgel 60, no. 9385, 230–400 mesh ASTM). ¹H and ¹³C NMR spectra were obtained with a Varian Mercury-300 or Varian Mercury-400 spectrometers. Chemical shifts were recorded in parts per million (ppm, δ) and were reported relative to the solvent peak or TMS. Low-resolution mass spectra (LRMS) data were measured on an Agilent MSD-1100 ESI-MS/MS system. High-resolution mass spectra (HRMS) were measured with a VARIAN 901-MS (FT-ICR Mass) mass spectrometer. Purity of the final compounds was determined using a Hitachi 2000 series HPLC system equipped with a C-18 column (Agilent ZORBAX Eclipse XDB-C18 5 μ m, 4.6 mm × 150 mm), using mobile phase A-acetonitrile and mobile phase B-water

containing 0.1% formic acid + 10 mmol NH₄OAc. Elution condition: 0 min phase A 10% + phase B 90%; at 45 min phase A 90% + phase B 10%; at 50 min phase A 10% + phase B 90%; at 60 min phase A 10% + phase B 90%. The flow-rate was 0.5 mL/min, and the injection volume was 5 μ L. The system was operated at 25 °C. Peaks were detected at 254 nm. IUPAC nomenclatures of compounds were performed by ACD/Name Pro software. A JASCO P-1020 polarimeter with a sodium lamp was used for the determination of specific rotation at 20 °C.

4,5-Dichloro-6-phenylfuro[2,3-*d*]pyrimidine (1b). Compounds **1b** was prepared from **1a** and *N*-chlorosuccinimide, in a manner similar to **1c** reported by us. ¹H NMR (400 MHz, CDCl₃) δ 7.24–7.60 (m, 3 H), 8.15–8.19 (m, 3 H), 8.78 (s, 1 H). LCMS (ESI) *m/z* 264 ([M + H]⁺). Purity 99.23% (*T_R* = 42.62 min)³⁸

(2S)-2-[(5-Bromo-6-phenylfuro[2,3-*d*]pyrimidin-4-yl)amino]-2-phenylethanol (2f). To a solution of compound **1c** (20.0 g, 64.6 mmol) in EtOH (300 mL) was added Et₃N (10 mL) and (S)-(+)-2-phenylglycinol (9.6 g, 70.0 mmol) and refluxed for overnight. After cooling to room temperature, the reaction mixture was concentrated and the residue was purified by silica gel column chromatography using a mixture of CH₂Cl₂/MeOH (40:1) to give **2f** (25.86 g, 98%) as a pale-yellow solid. ¹H NMR (300 MHz, CDCl₃) δ 3.99–4.13 (m, 2 H), 5.50 (dt, *J* = 6.6, 4.8 Hz, 1 H), 6.91 (d, *J* = 6.6 Hz, 1 H), 7.30–7.56 (m, 8 H), 8.06 (dt, *J* = 6.6, 1.8 Hz, 2 H), 8.34 (s, 1 H).

[α]_D²⁰ = −223.96° (*c* = 0.25 in CH₂Cl₂). LCMS (ESI) *m/z* 410 ([M + H]⁺). HRMS (EI) calcd for C₂₀H₁₆BrN₃O₂ (M⁺) 409.0426, found 409.0412. Purity 100.00% (*T_R* = 36.90 min). Compounds **2a–e** were prepared from **1a–b** and corresponding amines in 85–98% yield in a manner similar to **2f**.

(2S)-2-[(5,6-Diphenylfuro[2,3-*d*]pyrimidin-4-yl)amino]-2-phenylethanol (2a). A mixture of EtOAc/*n*-hexane (1:3) was used as the eluent. ¹H NMR (300 MHz, CDCl₃) δ 3.67–3.90 (m, 2 H), 5.26 (td, *J* = 6.3, 3.6 Hz, 1 H), 5.35 (d, *J* = 6.3 Hz, 1 H), 6.93–7.09 (m, 2 H), 7.23–7.32 (m, 5 H), 7.47 (br, 5 H), 7.51–7.67 (m, 3 H), 8.37–8.43 (m, 1 H). [α]_D²⁰ = −182.04° (*c* = 0.25 in CH₂Cl₂). LCMS (ESI) *m/z* 408 ([M + H]⁺). HRMS (ESI) calcd for C₂₆H₂₂N₃O₂ ([M + H]⁺) 408.1712, found 408.1706. Purity 100.00% (*T_R* = 38.84 min).

5,6-Diphenyl-*N*-[(1*R*)-1-phenylethyl]furo[2,3-*d*]pyrimidin-4-amine (2b). A mixture of EtOAc/*n*-hexane (1:5) was used as the eluent. ¹H NMR (300 MHz, CDCl₃) δ 1.28 (d, *J* = 6.9 Hz, 3 H), 4.85 (d, *J* = 7.5 Hz, 1 H), 5.29–5.34 (m, 1 H), 7.01 (d, *J* = 7.5 Hz, 2 H), 7.12–7.25 (m, 6 H), 7.36–7.52 (m, 7 H), 8.31 (s, 1 H). [α]_D²⁰ = −27.46° (*c* = 0.255 in CH₂Cl₂). LCMS (ESI) *m/z* 392 ([M + H]⁺). HRMS (ESI) calcd for C₂₆H₂₂N₃O ([M + H]⁺) 392.1763, found 392.1751. Purity 99.27% (*T_R* = 48.69 min).

5,6-Diphenyl-*N*-[(1*R*)-1-phenylpropyl]furo[2,3-*d*]pyrimidin-4-amine (2c). A mixture of EtOAc/*n*-hexane (1:5) was used as the eluent. ¹H NMR (300 MHz, CDCl₃) δ 0.72 (t, *J* = 7.2 Hz, 3 H), 1.64 (quintet, *J* = 7.2 Hz, 3 H), 4.98 (d, *J* = 8.1 Hz, 1 H), 5.11–5.22 (m, 1 H), 7.04 (d, *J* = 8.1 Hz, 2 H), 7.15–7.34 (m, 6 H), 7.46–7.68 (m, 7 H), 8.36 (s, 1 H). LCMS (ESI) *m/z* 406 ([M + H]⁺). HRMS (ESI) calcd for C₂₇H₂₄N₃O ([M + H]⁺) 406.1919, found 406.1923. Purity 96.89% (*T_R* = 50.65 min).

Methyl (2S)-[(5,6-Diphenylfuro[2,3-*d*]pyrimidin-4-yl)amino]-(phenyl)ethanoate (2d). A mixture of EtOAc/*n*-hexane (1:4) was used as the eluent. ¹H NMR (300 MHz, CDCl₃) δ 3.67 (s, 3 H), 5.64–5.75 (m, 1 H), 5.70 (d, *J* = 7.2 Hz, 1 H), 5.83 (d, *J* = 7.2 Hz, 1 H), 7.17–7.36 (m, 8 H), 7.46–7.65 (m, 7 H), 8.39 (s, 1 H). [α]_D²⁰ = −26.68° (*c* = 0.25 in CH₂Cl₂). LCMS (ESI) *m/z* 436 ([M + H]⁺). HRMS (ESI) calcd for C₂₇H₂₂N₃O₃ ([M + H]⁺) 436.1661, found 436.1643. Purity 92.40% (*T_R* = 38.84 min).

(2S)-2-[(5-Chloro-6-phenylfuro[2,3-*d*]pyrimidin-4-yl)amino]-2-phenylethanol (2e). A mixture of EtOAc/*n*-hexane (1:4) was used as the eluent. ¹H NMR (300 MHz, CDCl₃) δ 4.07 (t, *J* = 4.5 Hz, 2 H), 5.44–5.56 (m, 1 H), 6.64 (d, *J* = 6.6 Hz, 1 H), 7.33–7.40 (m, 1 H), 7.40–7.55 (m, 7 H), 8.05 (dd, *J* = 8.2, 1.2 Hz, 2 H), 8.35 (s, 1 H). LCMS (ESI) *m/z* 366 ([M + H]⁺). HRMS (ESI) calcd for C₂₀H₁₇ClN₃O₂ ([M + H]⁺) 366.1009, found 366.1005. Purity 100.00% (*T_R* = 36.51 min).

(2S)-2-[[5-(3-Nitrophenyl)-6-phenylfuro[2,3-d]pyrimidin-4-yl]amino]-2-phenylethanol (3d). To a solution of compound **2f** (34.95 g, 85.19 mmol) in dioxane (450 mL) and H₂O (50 mL) was added 3-nitrophenylboronic acid (21.33 g, 127.78 mmol), Na₂CO₃ (13.54 g, 127.78 mmol), and Pd(dppf)Cl₂ (6.23 g, 8.52 mmol). The mixture was degassed and then stirred at 100 °C under Ar(g) for 2 h. After cooling to rt, solvents were removed under reduced pressure, and H₂O and CH₂Cl₂ were added to partition. Organic layers were collected, dried over MgSO₄, filtered, and concentrated, and the residue was purified by silica gel column chromatography using a mixture of CH₂Cl₂/MeOH (40:1) to give **3d** (25.86 g, 98%) as a pale-yellow solid. Compounds **3a–c,e–g** were prepared from **2f** and corresponding boronic acid in 60–95% yield in a manner similar to **3d**. ¹H NMR (400 MHz, CDCl₃) δ 3.27 (t, *J* = 5.6 Hz, 1 H), 3.85 (t, *J* = 4.8 Hz, 2 H), 5.16–5.28 (m, 2 H), 7.05–7.13 (m, 2 H), 7.27–7.37 (m, 6 H), 7.46–7.53 (m, 2 H), 7.65 (t, *J* = 8.0 Hz, 1 H), 7.82 (d, *J* = 7.6 Hz, 1 H), 8.30 (ddd, *J* = 8.0, 2.4, 1.2 Hz, 1 H), 8.40 (s, 1 H), 8.41 (s, 1 H). [α]_D²⁰ = –226.92° (*c* = 0.25 in CH₂Cl₂). LCMS (ESI) *m/z*: 453 ([M + H]⁺), 475 ([M + Na]⁺). HRMS (EI) calcd for C₂₆H₂₀N₄O₄ (M⁺) 452.1485, found 452.1491. Purity 99.78% (*T_R* = 37.73 min).

(2S)-2-[[5-(Furan-2-yl)-6-phenylfuro[2,3-d]pyrimidin-4-yl]amino]-2-phenylethanol (3a). A mixture of EtOAc/*n*-hexane (1:3) was used as the eluent. ¹H NMR (300 MHz, CDCl₃) δ 3.97–4.02 (m, 2 H), 5.37 (td, *J* = 5.7, 3.9 Hz, H), 6.46–6.54 (m, 2 H), 6.89 (d, *J* = 5.7 Hz, 1 H), 7.28–7.50 (m, 9 H), 7.66–7.77 (m, 2 H), 8.38 (s, 1 H). [α]_D²⁰ = –158.12° (*c* = 0.25 in CH₂Cl₂). LCMS (ESI) *m/z*: 398 ([M + H]⁺). Purity 99.03% (*T_R* = 37.11 min).

(2S)-2-[[5-(Furan-3-yl)-6-phenylfuro[2,3-d]pyrimidin-4-yl]amino]-2-phenylethanol (3b). A mixture of EtOAc/*n*-hexane (1:3) was used as the eluent. ¹H NMR (300 MHz, CDCl₃) δ 3.84–3.96 (m, 2 H), 5.30 (q, *J* = 5.4 Hz, 1 H), 5.76 (d, *J* = 6.3 Hz, 1 H), 6.51–6.58 (m, 1 H), 7.13–7.23 (m, 2 H), 7.27–7.41 (m, 6 H), 7.58–7.65 (m, 2 H), 7.65–7.77 (m, 3 H), 8.37 (s, 1 H). [α]_D²⁰ = –188.04° (*c* = 0.25 in CH₂Cl₂). LCMS (ESI) *m/z*: 398 ([M + H]⁺). HRMS (ESI) calcd for C₂₄H₂₀N₃O₃ ([M + H]⁺) 398.1505, found 398.1494. Purity 100.00% (*T_R* = 36.11 min).

(2S)-2-[[5-(1,3-Benzodioxol-5-yl)-6-phenylfuro[2,3-d]pyrimidin-4-yl]amino]-2-phenylethanol (3c). A mixture of EtOAc/*n*-hexane (1:3) was used as the eluent. ¹H NMR (300 MHz, CDCl₃) δ: 3.85 (d, *J* = 4.8 Hz, 2 H), 4.18 (br, 1 H), 5.20 (q, *J* = 5.1 Hz, 1 H), 5.46 (d, *J* = 4.8 Hz, 1 H), 5.72–6.13 (m, 2 H), 6.9 (br, 3 H), 7.06–7.14 (m, 2 H), 7.27–7.38 (m, 6 H), 7.53–7.67 (m, 2 H), 8.36 (s, 1 H). LCMS (ESI) *m/z*: 452 ([M + H]⁺). HRMS (ESI) calcd for C₂₇H₂₂N₃O₄ ([M + H]⁺) 452.1610, found 452.1596. Purity 95.02% (*T_R* = 37.85 min).

(2S)-2-[[5-(3-Aminophenyl)-6-phenylfuro[2,3-d]pyrimidin-4-yl]amino]-2-phenylethanol (3e). A mixture of MeOH/CH₂Cl₂ (1:30) was used as the eluent. ¹H NMR (400 MHz, CDCl₃) δ 3.69–4.00 (m, 4 H), 5.26 (td, *J* = 6.4, 3.6 Hz, 1 H), 5.62 (d, *J* = 5.2 Hz, 1 H), 6.74 (dd, *J* = 8.0, 1.2 Hz, 2 H), 7.06–7.11 (m, 2 H), 7.27–7.34 (m, 8 H), 7.63 (dd, *J* = 7.6, 1.6 Hz, 2 H), 8.36 (s, 1 H). [α]_D²⁰ = –185.04° (*c* = 0.25 in CH₂Cl₂). LCMS (ESI) *m/z*: 423 ([M + H]⁺). HRMS (EI) calcd for C₂₆H₂₂N₄O₂ (M⁺) 422.1743, found 422.1728. Purity 99.83% (*T_R* = 37.57 min).

N-[4-(4-[[[(1S)-2-Hydroxy-1-phenylethyl]amino]-6-phenylfuro[2,3-d]pyrimidin-5-yl]phenyl]acetamide (3f). A mixture of EtOAc/*n*-hexane (1:3) was used as the eluent. ¹H NMR (300 MHz, CDCl₃) δ 2.25 (s, 3 H), 3.58–3.92 (m, 3 H), 5.15–5.25 (m, 1 H), 5.42 (d, *J* = 6.3 Hz, 1 H), 7.04–7.11 (m, 2 H), 7.22–7.36 (m, 5 H), 7.46 (d, *J* = 8.1 Hz, 2 H), 7.58 (dd, *J* = 6.6, 3.0 Hz, 5 H), 8.36 (s, 1 H). LCMS (ESI) *m/z*: 465 ([M + H]⁺). HRMS (ESI) calcd for C₂₈H₂₅N₄O₃ ([M + H]⁺) 465.1927, found 465.1918. Purity 99.09% (*T_R* = 30.46 min).

N-[3-(4-[[[(1S)-2-Hydroxy-1-phenylethyl]amino]-6-phenylfuro[2,3-d]pyrimidin-5-yl]phenyl]acetamide (3g). A mixture of EtOAc/*n*-hexane (1:3) was used as the eluent. ¹H NMR (400 MHz, CDCl₃) δ 2.16 (br, 3 H), 3.73 (dd, *J* = 11.2, 6.4 Hz, 1 H), 3.87 (dd, *J* = 11.2, 2.4 Hz, 1 H), 5.32 (br, 1 H), 5.58 (br, 1 H), 7.05 (dd, *J* = 7.2, 2.4 Hz, 2 H), 7.17–7.30 (m, 7 H), 7.42 (t, *J* = 7.6 Hz, 1 H), 7.49–7.56 (m, 2 H), 7.57–7.71 (m, 2 H), 8.33 (s, 1 H). [α]_D²⁰ = –283.32°

(*c* = 0.25 in CH₂Cl₂). LCMS (ESI) *m/z*: 465 ([M + H]⁺). HRMS (ESI) calcd for C₂₈H₂₅N₄O₃ ([M + H]⁺) 465.1927, found 465.1915. Purity 100.00% (*T_R* = 31.00 min).

N-[3-(4-[[[(1S)-2-Hydroxy-1-phenylethyl]amino]-6-phenylfuro[2,3-d]pyrimidin-5-yl]phenyl]-N²,N²-dimethylglycinamide (4a). To a solution of **3e** (104 mg, 0.25 mmol) in dry CH₂Cl₂ (5 mL) was added EDCI (80 mg, 0.42 mmol) and 2-(dimethylamino)acetic acid (60 mg, 0.58 mmol) and stirred at rt for 16 h. After the reaction was completed, H₂O and CH₂Cl₂ were added to partition. Organic layers were collected, dried over MgSO₄, filtered, and concentrated, and the residue was purified by silica gel column chromatography using a mixture of CH₂Cl₂/MeOH (40:1) to give **4a** (85 mg, 65%) as a white solid. Compounds **4b–f** were prepared from **3e** and corresponding carboxylic acid, in 45–73% yield in a manner similar to **4a**. ¹H NMR (400 MHz, CDCl₃) δ 2.34 (s, 6 H), 3.06 (br, 2 H), 3.73 (dd, *J* = 11.2, 6.4 Hz, 1 H), 3.84 (dd, *J* = 11.2, 2.8 Hz, 1 H), 5.31 (br, 1 H), 5.55 (br, 1 H), 7.03 (dd, *J* = 7.6, 1.6 Hz, 2 H), 7.17–7.31 (m, 7 H), 7.44 (t, *J* = 7.2 Hz, 1 H), 7.45–7.91 (m, 2 H), 7.69 (m, 2 H), 8.35 (s, 1 H), 9.21 (br, 1 H). [α]_D²⁰ = –25.24° (*c* = 0.25 in CH₂Cl₂). LCMS (ESI) *m/z*: 508 ([M + H]⁺). HRMS (ESI) calcd for C₃₀H₃₀N₅O₃ ([M + H]⁺) 508.2349, found 508.2342. Purity 97.74% (*T_R* = 22.64 min).

N-[3-(4-[[[(1S)-2-Hydroxy-1-phenylethyl]amino]-6-phenylfuro[2,3-d]pyrimidin-5-yl]phenyl]-N³,N³-dimethyl-β-alaninamide (4b). A mixture of MeOH/CH₂Cl₂ (1:25) was used as the eluent. ¹H NMR (400 MHz, CDCl₃) δ 2.26 (br, 6 H), 2.43 (br, 3 H), 2.58 (br, 3 H), 3.66 (dd, *J* = 11.2, 6.0 Hz, 1 H), 3.80 (d, *J* = 11.2 Hz, 1 H), 5.28 (br, 1H), 5.61 (br, 1 H), 6.92–7.04 (m, 2 H), 7.07–7.26 (m, 9 H), 7.34 (t, *J* = 7.2 Hz, 1 H), 7.47–7.55 (m, 2 H), 7.72 (br, 1 H), 8.29 (s, 1 H). [α]_D²⁰ = –269.04° (*c* = 0.25 in CH₂Cl₂). LCMS (ESI) *m/z*: 522 ([M + H]⁺). HRMS (ESI) calcd for C₃₁H₃₂N₅O₃ ([M + H]⁺) 522.2505, found 522.2505. Purity 99.56% (*T_R* = 23.17 min).

4-(Dimethylamino)-N-[3-(4-[[[(1S)-2-hydroxy-1-phenylethyl]amino]-6-phenylfuro[2,3-d]pyrimidin-5-yl]phenyl]butanamide (4c). A mixture of MeOH/CH₂Cl₂ (1:30) was used as the eluent. ¹H NMR (400 MHz, CD₃OD) δ 1.90 (quintet, *J* = 7.6 Hz, 2 H), 2.27 (s, 6 H), 2.37–2.48 (m, 4 H), 3.64 (dd, *J* = 11.2, 5.2 Hz, 1 H), 3.77 (dd, *J* = 11.2, 5.2 Hz, 1 H), 5.29 (t, *J* = 5.2 Hz, 1 H), 7.14–7.20 (m, 2 H), 7.21–7.39 (m, 8 H), 7.53–7.63 (m, 3 H), 7.79 (ddd, *J* = 8.4, 2.4, 0.8 Hz, 1 H), 7.92 (t, *J* = 1.6 Hz, 1 H), 8.27 (s, 1 H). LCMS (ESI) *m/z*: 536 ([M + H]⁺). HRMS (ESI) calcd for C₃₂H₃₄N₅O₃ ([M + H]⁺) 536.2662, found 536.2642. Purity 88.82% (*T_R* = 23.03 min).

5-(Dimethylamino)-N-[3-(4-[[[(1S)-2-hydroxy-1-phenylethyl]amino]-6-phenylfuro[2,3-d]pyrimidin-5-yl]phenyl]pentanamide (4d). A mixture of MeOH/CH₂Cl₂ (1:30) was used as the eluent. ¹H NMR (400 MHz, CDCl₃) δ 1.38–1.49 (m, 2 H), 1.56–1.72 (m, 2 H), 1.86 (s, 7 H), 2.02–2.19 (m, 2 H), 2.28 (t, *J* = 7.2 Hz, 2 H), 3.57 (dd, *J* = 11.2, 4.4 Hz, 1 H), 3.66 (dd, *J* = 11.2, 3.2 Hz, 1 H), 5.09–5.19 (m, 1 H), 5.83 (d, *J* = 7.2 Hz, 1 H), 7.02 (d, *J* = 7.2 Hz, 2 H), 7.13 (t, *J* = 7.2 Hz, 2 H), 7.16–7.24 (m, 6 H), 7.35 (t, *J* = 8.0 Hz, 1 H), 7.42–7.54 (m, 3 H), 7.92 (d, *J* = 5.6 Hz, 1 H), 8.28 (s, 1 H), 8.73 (br, 1 H). [α]_D²⁰ = –29.12° (*c* = 0.245 in CH₂Cl₂). LCMS (ESI) *m/z*: 550 ([M + H]⁺). HRMS (ESI) calcd for C₃₃H₃₆N₅O₃ ([M + H]⁺) 550.2818, found 550.2824. Purity 97.96% (*T_R* = 23.37 min).

6-(Dimethylamino)-N-[3-(4-[[[(1S)-2-hydroxy-1-phenylethyl]amino]-6-phenylfuro[2,3-d]pyrimidin-5-yl]phenyl]hexanamide (4e). A mixture of MeOH/CH₂Cl₂ (1:30) was used as the eluent. ¹H NMR (400 MHz, DMSO-*d*₆) δ 1.20–1.44 (m, 4 H), 1.58 (quintet, *J* = 7.2 Hz, 2 H), 2.06 (s, 6 H), 2.13 (t, *J* = 7.2 Hz, 2 H), 2.31 (t, *J* = 7.2 Hz, 2 H), 3.38–3.47 (m, 1 H), 3.54–3.62 (m, 1 H), 4.85 (t, *J* = 4.8 Hz, 1 H), 5.19 (dd, *J* = 12.4, 4.4 Hz, 1 H), 5.72 (d, *J* = 7.6 Hz, 1 H), 7.10–7.29 (m, 6 H), 7.30–7.43 (m, 3 H), 7.47–7.59 (m, 3 H), 7.74 (d, *J* = 8.8 Hz, 1 H), 7.86–7.99 (m, 1 H), 8.23–8.32 (m, 1 H), 10.03–10.15 (m, 1 H). [α]_D²⁰ = –302.56° (*c* = 0.25 in CH₂Cl₂). LCMS (ESI) *m/z*: 564 ([M + H]⁺). Purity 94.15% (*T_R* = 40.18 min).

N-[3-(4-[[[(1S)-2-Hydroxy-1-phenylethyl]amino]-6-phenylfuro[2,3-d]pyrimidin-5-yl]phenyl]-5-methylhexanamide (4f). A mixture of EtOAc/*n*-hexane (2:3) was used as the eluent. ¹H NMR (400 MHz, CDCl₃) δ 0.89 (d, *J* = 6.8 Hz, 6H), 1.30–1.20 (m, 2H), 1.77–1.50 (m, 3H), 2.33 (br, 2H), 3.78–3.68 (m, 1H), 3.92–3.82 (m, 1H), 5.35 (br. s., 1H), 5.59 (br, 1H), 7.06 (d, *J* = 7.6 Hz, 2H),

7.34–7.18 (m, 9H), 7.42 (t, $J = 7.6$ Hz, 1H), 7.82–7.52 (m, 3H), 8.37 (s, 1H). $[\alpha]_D^{20} = -261.84^\circ$ ($c = 0.25$ in CH_2Cl_2). LCMS (ESI) m/z 535 ($[\text{M} + \text{H}]^+$), 557 ($[\text{M} + \text{Na}]^+$). HRMS (ESI) calcd for $\text{C}_{33}\text{H}_{35}\text{N}_4\text{O}_3$ ($[\text{M} + \text{H}]^+$) 535.2709, found 535.2711. Purity 100.0% ($T_R = 43.66$ min).

EGFR Kinase Assay. Wild-type and L834R mutant of human EGFR kinase domain were amplified by PCR and subcloned to pBac-PAK8-GST-EGFR-KD plasmid for generating recombinant baculovirus for protein expression in *Spodoptera frugiperda* Sf9 cells, separately. The GST fusion proteins were expressed and purified as described previously.⁶⁵ Kinase-Glo luminescent kinase assay was used for determining wild-type and L834R mutant EGFR kinase activity. The assay was first done at 30 °C for 2 h in a 96-well plates with a final volume of 50 μL containing 200 ng of wild-type GST-fusion proteins, 25 mM HEPES, pH 7.4, 4 mM MnCl_2 , 2 mM DTT, 10 mM MgCl_2 , 0.01% bovine serum albumin, 0.02% Triton X-100, 5 μM poly-(Glu,Tyr) 4:1, 0.5 mM Na_2VO_4 , and 10 μM ATP. After incubation, 50 μL of Kinase-Glo Plus reagent (Promega) was added and further incubated at 25 °C for 20 min. Then a 70 μL aliquot of each reaction mixture was transferred to a black microtiter plate and measured the luminescence by a Wallac Vector 1420 multilabel counter (Perkin-Elmer).

Protein Purification and Crystallography. Co-crystal complex structure determinations were carried out as previously described.³⁸ Human EGFR kinase domain were expressed and purified by using a baculovirus/insect cell system. The amplified DNA was subcloned into pBacPAK8-MT-EGFP-GST vector to generate recombinant baculovirus for protein expression. The recombinant protein was large scale production in Hi5 insect cells. The cell pellets were suspended in tris-buffer solution (50 mM Tris-Cl pH8.0, 1 mM DTT) and lysed by sonication. Cell debris was removed by centrifugation at 19000 rpm for 30 min at 4 °C, and supernatant was collected for further purification. The protein was purified by GST affinity column by washed with 1 \times PBS buffer and eluted with 20 mM GSH in 50 mM Tris-Cl (pH8.0) buffer solution. The eluted protein was exchanged to PreScission protease digestion buffer (50 mM Tris-Cl, 150 mM NaCl, 1 mM EDTA, 1 mM DTT, pH8.0) by desalting column and digested with PreScission protease (GE Healthcare) at 4 °C for 16 h. The GST tag was removed by loading the digested mixture to the second GST affinity column and recovered the fractions of flow-through. The flow-through was then buffer exchanged to final buffer [20 mM Tris-Cl (pH8.0), 100 mM sodium chloride, and 5 mM DTT] and concentrated up to 4–6 mg/mL and flash-frozen in liquid nitrogen for storage at –80 °C.

The purified EGFR kinase domain (4–6 mg/mL) was crystallized by hanging drop vapor diffusion method. The crystals were grown at 18 °C for 3–7 days. The complex crystals were obtained by soaking apo crystals in reservoir solution (1.0 M ammonium citrate tribase, pH7.0, 0.1 M Bis-Tris propane, pH 7.0) containing 0.6–1.0 mM compound. The complex crystals were immersed briefly in 14.3–22.2% glycerol in soaking drop before being flash-frozen in liquid nitrogen. Diffraction data were collected at the NSRRC (beamline BL13B1 and BL13C1) and SPring8 synchrotron facility (beamline BL12B2). The structures were solved by the molecular replacement method MOLREP⁶⁶ of the CCP4 program suite⁶⁷ using the EGFR structure (PDB code: 1M17) as a search model. The structures were refined by utilizing REFMAC⁶⁸ followed by model building with program O⁶⁹ and AFITT (OpenEye Scientific Software, USA). The completed structure model was optimized by using a PDB_REDO.⁷⁰ The final models were validated using Molprobit.⁷¹ All structural figures were generated using PyMOL (Schrödinger, USA).

■ ASSOCIATED CONTENT

■ Supporting Information

Data collection and refinement statistics for X-ray crystallography, kinase profiling of compound **4b**, overlay of EGFR/**4b** structure with JAK1 and CDK2. This material is available free of charge via the Internet at <http://pubs.acs.org>.

Accession Codes

4JQ7, 4JQ8, 4JR3, 4JRV.

■ AUTHOR INFORMATION

Corresponding Author

*For S.Y.W.: phone, +886-37-246-166 extension 35713; fax, +886-37-586-456; E-mail, suying@nhri.org.tw. For H.P.H.: phone, +886-37-246-166 extension 35708; fax, +886-37-586-456; E-mail, hphsieh@nhri.org.tw.

Author Contributions

^{||}These authors contributed equally.

Notes

The authors declare no competing financial interest.

■ ACKNOWLEDGMENTS

Grant support was from the National Health Research Institute, Taiwan, ROC, and the National Science Council (grant no. NSC-101-2321-B-400-005 for Drs. Y.S.C. and H.P.H., NSC-101-2113-M-400-002-MY4 for H.P.H., and NSC 99-2113-M-400-002-MY3 for H.Y.S.). We thank the staff of beamline BL13B1 and BL13C1 at National Synchrotron Radiation Research Centre (NSRRC), Taiwan, and BL12B2 at SPring-8, Japan, for technical assistance. We also thank Mark Swofford for helping with the English editing.

■ ABBREVIATIONS USED

EGFR, epidermal growth factor receptor; NSCLC, non-small cell lung cancer; ATP, adenosine triphosphate; SBDD, structure-based drug design; DFG, Asp-Phe-Gly; TKIs, tyrosine kinase inhibitors; ILD, interstitial lung disease; STK10, serine/threonine kinase 10; EPHA3, erythropoietin-producing human hepatocellular carcinoma receptor A3; CDC7, cell division cycle 7-related protein kinase; JAK1, Janus kinase 1; CDK2, cyclin-dependent kinase 2

■ REFERENCES

- (1) Manning, G.; Whyte, D. B.; Martinez, R.; Hunter, T.; Sudarsanam, S. The protein kinase complement of the human genome. *Science* **2002**, *298*, 1912–1934.
- (2) Zuccotto, F.; Ardini, E.; Casale, E.; Angiolini, M. Through the “gatekeeper door”: exploiting the active kinase conformation. *J. Med. Chem.* **2010**, *53*, 2681–2694.
- (3) Zhang, J.; Yang, P. L.; Gray, N. S. Targeting cancer with small molecule kinase inhibitors. *Nature Rev. Cancer* **2009**, *9*, 28–39.
- (4) Huse, M.; Kuriyan, J. The conformational plasticity of protein kinases. *Cell* **2002**, *109*, 275–282.
- (5) Nagar, B. c-Abl tyrosine kinase and inhibition by the cancer drug imatinib (Gleevec/STI-571). *J. Nutr.* **2007**, *137*, 1518S–1523S.
- (6) Hubbard, S. R. Crystal structure of the activated insulin receptor tyrosine kinase in complex with peptide substrate and ATP analog. *EMBO J.* **1997**, *16*, 5572–5581.
- (7) Hubbard, S. R.; Wei, L.; Ellis, L.; Hendrickson, W. A. Crystal structure of the tyrosine kinase domain of the human insulin receptor. *Nature* **1994**, *372*, 746–754.
- (8) Sicheri, F.; Moarefi, I.; Kuriyan, J. Crystal structure of the Src family tyrosine kinase Hck. *Nature* **1997**, *385*, 602–609.
- (9) Schlessinger, J. Common and distinct elements in cellular signaling via EGF and FGF receptors. *Science* **2004**, *306*, 1506–1507.
- (10) Hynes, N. E.; MacDonald, G. ErbB receptors and signaling pathways in cancer. *Curr. Opin. Cell Biol.* **2009**, *21*, 177–184.
- (11) Ernst, E. Mistletoe for cancer? *Eur. J. Cancer* **2001**, *37*, 9–11.
- (12) Klapper, L. N.; Kirschbaum, M. H.; Sela, M.; Yarden, Y. Biochemical and clinical implications of the ErbB/HER signaling network of growth factor receptors. *Adv. Cancer Res.* **2000**, *77*, 25–79.

- (13) Olayioye, M. A.; Neve, R. M.; Lane, H. A.; Hynes, N. E. The ErbB signaling network: receptor heterodimerization in development and cancer. *EMBO J.* **2000**, *19*, 3159–3167.
- (14) Stamos, J.; Sliwkowski, M. X.; Eigenbrot, C. Structure of the epidermal growth factor receptor kinase domain alone and in complex with a 4-anilinoquinazoline inhibitor. *J. Biol. Chem.* **2002**, *277*, 46265–46272.
- (15) Kim, S.; Prichard, C. N.; Younes, M. N.; Yazici, Y. D.; Jasser, S. A.; Bekele, B. N.; Myers, J. N. Cetuximab and irinotecan interact synergistically to inhibit the growth of orthotopic anaplastic thyroid carcinoma xenografts in nude mice. *Clin. Cancer Res.* **2006**, *12*, 600–607.
- (16) Baselga, J.; Averbuch, S. D. ZD1839 ('Iressa') as an anticancer agent. *Drugs* **2000**, *60*, 33–40.
- (17) Yun, C. H.; Boggon, T. J.; Li, Y.; Woo, M. S.; Greulich, H.; Meyerson, M.; Eck, M. J. Structures of lung cancer-derived EGFR mutants and inhibitor complexes: mechanism of activation and insights into differential inhibitor sensitivity. *Cancer Cell* **2007**, *11*, 217–227.
- (18) Rusnak, D. W.; Lackey, K.; Affleck, K.; Wood, E. R.; Allgood, K. J.; Rhodes, N.; Keith, B. R.; Murray, D. M.; Knight, W. B.; Mullin, R. J.; Gilmer, T. M. The effects of the novel, reversible epidermal growth factor receptor/ErbB-2 tyrosine kinase inhibitor, GW2016, on the growth of human normal and tumor-derived cell lines in vitro and in vivo. *Mol. Cancer Ther.* **2001**, *1*, 85–94.
- (19) Wood, E. R.; Truesdale, A. T.; McDonald, O. B.; Yuan, D.; Hassell, A.; Dickerson, S. H.; Ellis, B.; Pennisi, C.; Horne, E.; Lackey, K.; Allgood, K. J.; Rusnak, D. W.; Gilmer, T. M.; Shewchuk, L. A unique structure for epidermal growth factor receptor bound to GW572016 (Lapatinib): relationships among protein conformation, inhibitor off-rate, and receptor activity in tumor cells. *Cancer Res.* **2004**, *64*, 6652–6659.
- (20) Yokoi, K.; Thaker, P. H.; Yazici, S.; Rebhun, R. R.; Nam, D. H.; He, J.; Kim, S. J.; Abbruzzese, J. L.; Hamilton, S. R.; Fidler, I. J. Dual inhibition of epidermal growth factor receptor and vascular endothelial growth factor receptor phosphorylation by AEE788 reduces growth and metastasis of human colon carcinoma in an orthotopic nude mouse model. *Cancer Res.* **2005**, *65*, 3716–3725.
- (21) Wong, T. W.; Lee, F. Y.; Yu, C.; Luo, F. R.; Oppenheimer, S.; Zhang, H.; Smykla, R. A.; Mastalerz, H.; Fink, B. E.; Hunt, J. T.; Gavai, A. V.; Vite, G. D. Preclinical antitumor activity of BMS-599626, a pan-HER kinase inhibitor that inhibits HER1/HER2 homodimer and heterodimer signaling. *Clin. Cancer Res.* **2006**, *12*, 6186–6193.
- (22) Aertgeerts, K.; Skene, R.; Yano, J.; Sang, B. C.; Zou, H.; Snell, G.; Jennings, A.; Iwamoto, K.; Habuka, N.; Hirokawa, A.; Ishikawa, T.; Tanaka, T.; Miki, H.; Ohta, Y.; Sogabe, S. Structural analysis of the mechanism of inhibition and allosteric activation of the kinase domain of HER2 protein. *J. Biol. Chem.* **2011**, *286*, 18756–18765.
- (23) Ishikawa, T.; Seto, M.; Banno, H.; Kawakita, Y.; Oorui, M.; Taniguchi, T.; Ohta, Y.; Tamura, T.; Nakayama, A.; Miki, H.; Kamiguchi, H.; Tanaka, T.; Habuka, N.; Sogabe, S.; Yano, J.; Aertgeerts, K.; Kamiyama, K. Design and synthesis of novel human epidermal growth factor receptor 2 (HER2)/epidermal growth factor receptor (EGFR) dual inhibitors bearing a pyrrolo[3,2-*d*]pyrimidine scaffold. *J. Med. Chem.* **2011**, *54*, 8030–8050.
- (24) Rabindran, S. K.; Discafani, C. M.; Rosfjord, E. C.; Baxter, M.; Floyd, M. B.; Golas, J.; Hallett, W. A.; Johnson, B. D.; Nilakantan, R.; Overbeek, E.; Reich, M. F.; Shen, R.; Shi, X.; Tsou, H. R.; Wang, Y. F.; Wissner, A. Antitumor activity of HKI-272, an orally active, irreversible inhibitor of the HER-2 tyrosine kinase. *Cancer Res.* **2004**, *64*, 3958–3965.
- (25) Yun, C. H.; Mengwasser, K. E.; Toms, A. V.; Woo, M. S.; Greulich, H.; Wong, K. K.; Meyerson, M.; Eck, M. J. The T790M mutation in EGFR kinase causes drug resistance by increasing the affinity for ATP. *Proc. Natl. Acad. Sci. U S A.* **2008**, *105*, 2070–2075.
- (26) Zhou, W.; Ercan, D.; Chen, L.; Yun, C. H.; Li, D.; Capelletti, M.; Cortot, A. B.; Chiriac, L.; Iacob, R. E.; Padera, R.; Engen, J. R.; Wong, K. K.; Eck, M. J.; Gray, N. S.; Janne, P. A. Novel mutant-selective EGFR kinase inhibitors against EGFR T790M. *Nature* **2009**, *462*, 1070–1074.
- (27) Eskens, F. A.; Mom, C. H.; Planting, A. S.; Gietema, J. A.; Amelsberg, A.; Huisman, H.; van Doorn, L.; Burger, H.; Stopfer, P.; Verweij, J.; de Vries, E. G. A phase I dose escalation study of BIBW 2992, an irreversible dual inhibitor of epidermal growth factor receptor 1 (EGFR) and 2 (HER2) tyrosine kinase in a 2-week on, 2-week off schedule in patients with advanced solid tumours. *Br. J. Cancer* **2008**, *98*, 80–85.
- (28) Solca, F.; Dahl, G.; Zoephel, A.; Bader, G.; Sanderson, M.; Klein, C.; Kraemer, O.; Himmelsbach, F.; Haaksma, E.; Adolf, G. R. Target Binding Properties and Cellular Activity of Afatinib (BIBW 2992), an Irreversible ErbB Family Blocker. *J. Pharmacol. Exp. Ther.* **2012**, *343*, 342–350.
- (29) Kalous, O.; Conklin, D.; Desai, A. J.; O'Brien, N. A.; Ginther, C.; Anderson, L.; Cohen, D. J.; Britten, C. D.; Taylor, I.; Christensen, J. G.; Slamon, D. J.; Finn, R. S. Dacomitinib (PF-00299804), an irreversible Pan-HER inhibitor, inhibits proliferation of HER2-amplified breast cancer cell lines resistant to trastuzumab and lapatinib. *Mol. Cancer Ther.* **2012**, *11*, 1978–1987.
- (30) Ramalingam, S. S.; Blackhall, F.; Krzakowski, M.; Barrios, C. H.; Park, K.; Bover, I.; Seog Heo, D.; Rosell, R.; Talbot, D. C.; Frank, R.; Letrent, S. P.; Ruiz-Garcia, A.; Taylor, I.; Liang, J. Q.; Campbell, A. K.; O'Connell, J.; Boyer, M. Randomized phase II study of dacomitinib (PF-00299804), an irreversible pan-human epidermal growth factor receptor inhibitor, versus erlotinib in patients with advanced non-small-cell lung cancer. *J. Clin. Oncol.* **2012**, *30*, 3337–3344.
- (31) Chang, S. C.; Chang, C. Y.; Chang, S. J.; Yuan, M. K.; Lai, Y. C.; Liu, Y. C.; Chen, C. Y.; Kuo, L. C.; Yu, C. J. Gefitinib-Related Interstitial Lung Disease in Taiwanese Patients With Non-Small-Cell Lung Cancer. *Clin. Lung Cancer* **2012**, *14*, 55–61.
- (32) Widakowich, C.; de Castro, G., Jr.; de Azambuja, E.; Dinh, P.; Awada, A. Review: side effects of approved molecular targeted therapies in solid cancers. *Oncologist* **2007**, *12*, 1443–1455.
- (33) Castellino, S.; O'Mara, M.; Koch, K.; Borts, D. J.; Bowers, G. D.; MacLauchlin, C. Human metabolism of lapatinib, a dual kinase inhibitor: implications for hepatotoxicity. *Drug Metab. Dispos.* **2012**, *40*, 139–150.
- (34) Lovly, C. M.; Horn, L. Strategies for Overcoming EGFR Resistance in the Treatment of Advanced-Stage NSCLC. *Curr. Treat. Options Oncol.* **2012**, *13*, 516–526.
- (35) Yamamoto, N.; Honma, M.; Suzuki, H. Off-target serine/threonine kinase 10 inhibition by erlotinib enhances lymphocytic activity leading to severe skin disorders. *Mol. Pharmacol.* **2011**, *80*, 466–475.
- (36) Tsou, H. R.; Overbeek-Klumpers, E. G.; Hallett, W. A.; Reich, M. F.; Floyd, M. B.; Johnson, B. D.; Michalak, R. S.; Nilakantan, R.; Discafani, C.; Golas, J.; Rabindran, S. K.; Shen, R.; Shi, X.; Wang, Y. F.; Upeslakis, J.; Wissner, A. Optimization of 6,7-disubstituted-4-(arylamino)quinoline-3-carbonitriles as orally active, irreversible inhibitors of human epidermal growth factor receptor-2 kinase activity. *J. Med. Chem.* **2005**, *48*, 1107–1131.
- (37) Wood, E. R.; Truesdale, A. T.; McDonald, O. B.; Yuan, D.; Hassell, A.; Dickerson, S. H.; Ellis, B.; Pennisi, C.; Horne, E.; Lackey, K.; Allgood, K. J.; Rusnak, D. W.; Gilmer, T. M.; Shewchuk, L. A unique structure for epidermal growth factor receptor bound to GW572016 (Lapatinib): relationships among protein conformation, inhibitor off-rate, and receptor activity in tumor cells. *Cancer Res.* **2004**, *64*, 6652–6659.
- (38) Coumar, M. S.; Chu, C. Y.; Lin, C. W.; Shiao, H. Y.; Ho, Y. L.; Reddy, R.; Lin, W. H.; Chen, C. H.; Peng, Y. H.; Leou, J. S.; Lien, T. W.; Huang, C. T.; Fang, M. Y.; Wu, S. H.; Wu, J. S.; Chittimalla, S. K.; Song, J. S.; Hsu, J. T.; Wu, S. Y.; Liao, C. C.; Chao, Y. S.; Hsieh, H. P. Fast-forwarding hit to lead: aurora and epidermal growth factor receptor kinase inhibitor lead identification. *J. Med. Chem.* **2010**, *53*, 4980–4988.
- (39) Huang, S. F.; Liu, H. P.; Li, L. H.; Ku, Y. C.; Fu, Y. N.; Tsai, H. Y.; Chen, Y. T.; Lin, Y. F.; Chang, W. C.; Kuo, H. P.; Wu, Y. C.; Chen, Y. R.; Tsai, S. F. High frequency of epidermal growth factor receptor mutations with complex patterns in non-small cell lung cancers related

to gefitinib responsiveness in Taiwan. *Clin. Cancer Res.* **2004**, *10*, 8195–8203.

(40) Nagar, B.; Bornmann, W. G.; Pellicena, P.; Schindler, T.; Veach, D. R.; Miller, W. T.; Clarkson, B.; Kuriyan, J. Crystal structures of the kinase domain of c-Abl in complex with the small molecule inhibitors PD173955 and imatinib (STI-571). *Cancer Res.* **2002**, *62*, 4236–4243.

(41) Lawrence, H. R.; Martin, M. P.; Luo, Y.; Pireddu, R.; Yang, H.; Gevariya, H.; Ozcan, S.; Zhu, J. Y.; Kendig, R.; Rodriguez, M.; Elias, R.; Cheng, J. Q.; Sebt, S. M.; Schonbrunn, E.; Lawrence, N. J. Development of *o*-chlorophenyl substituted pyrimidines as exceptionally potent aurora kinase inhibitors. *J. Med. Chem.* **2012**, *55*, 7392–7416.

(42) Kuglstat, A.; Ghate, M.; Tsing, S.; Villasenor, A. G.; Shaw, D.; Barnett, J. W.; Browner, M. F. X-ray crystal structure of JNK2 complexed with the p38 α inhibitor BIRB796: insights into the rational design of DFG-out binding MAP kinase inhibitors. *Bioorg. Med. Chem. Lett.* **2010**, *20*, 5217–5220.

(43) Pargellis, C.; Tong, L.; Churchill, L.; Cirillo, P. F.; Gilmore, T.; Graham, A. G.; Grob, P. M.; Hickey, E. R.; Moss, N.; Pav, S.; Regan, J. Inhibition of p38 MAP kinase by utilizing a novel allosteric binding site. *Nature Struct. Biol.* **2002**, *9*, 268–272.

(44) Alevy, Y. G.; Patel, A. C.; Romero, A. G.; Patel, D. A.; Tucker, J.; Roswit, W. T.; Miller, C. A.; Heier, R. F.; Byers, D. E.; Brett, T. J.; Holtzman, M. J. IL-13-induced airway mucus production is attenuated by MAPK13 inhibition. *J. Clin. Invest.* **2012**, *122*, 4555–4568.

(45) Seeliger, M. A.; Ranjitkar, P.; Kasap, C.; Shan, Y.; Shaw, D. E.; Shah, N. P.; Kuriyan, J.; Maly, D. J. Equally potent inhibition of c-Src and Abl by compounds that recognize inactive kinase conformations. *Cancer Res.* **2009**, *69*, 2384–2392.

(46) Seeliger, M. A.; Nagar, B.; Frank, F.; Cao, X.; Henderson, M. N.; Kuriyan, J. c-Src binds to the cancer drug imatinib with an inactive Abl/c-Kit conformation and a distributed thermodynamic penalty. *Structure* **2007**, *15*, 299–311.

(47) Hodous, B. L.; Geuns-Meyer, S. D.; Hughes, P. E.; Albrecht, B. K.; Bellon, S.; Caenepeel, S.; Cee, V. J.; Chaffee, S. C.; Emery, M.; Fretland, J.; Gallant, P.; Gu, Y.; Johnson, R. E.; Kim, J. L.; Long, A. M.; Morrison, M.; Olivieri, P. R.; Patel, V. F.; Polverino, A.; Rose, P.; Wang, L.; Zhao, H. Synthesis, structural analysis, and SAR studies of triazine derivatives as potent, selective Tie-2 inhibitors. *Bioorg. Med. Chem. Lett.* **2007**, *17*, 2886–2889.

(48) Hodous, B. L.; Geuns-Meyer, S. D.; Hughes, P. E.; Albrecht, B. K.; Bellon, S.; Bready, J.; Caenepeel, S.; Cee, V. J.; Chaffee, S. C.; Coxon, A.; Emery, M.; Fretland, J.; Gallant, P.; Gu, Y.; Hoffman, D.; Johnson, R. E.; Kendall, R.; Kim, J. L.; Long, A. M.; Morrison, M.; Olivieri, P. R.; Patel, V. F.; Polverino, A.; Rose, P.; Tempest, P.; Wang, L.; Whittington, D. A.; Zhao, H. Evolution of a highly selective and potent 2-(pyridin-2-yl)-1,3,5-triazine Tie-2 kinase inhibitor. *J. Med. Chem.* **2007**, *50*, 611–626.

(49) Hughes, S.; Elustondo, F.; Di Fonzo, A.; Leroux, F. G.; Wong, A. C.; Snijders, A. P.; Matthews, S. J.; Cherepanov, P. Crystal structure of human CDC7 kinase in complex with its activator DBF4. *Nature Struct. Mol. Biol.* **2012**, *19*, 1101–1107.

(50) Echalié, A.; Cot, E.; Camasses, A.; Hodimont, E.; Hoh, F.; Jay, P.; Sheinerman, F.; Krasinska, L.; Fisher, D. An integrated chemical biology approach provides insight into Cdk2 functional redundancy and inhibitor sensitivity. *Chem. Biol.* **2012**, *19*, 1028–1040.

(51) Hole, A. J.; Baumli, S.; Shao, H.; Shi, S.; Huang, S.; Pepper, C.; Fischer, P. M.; Wang, S.; Endicott, J. A.; Noble, M. E. Comparative Structural and Functional Studies of 4-(Thiazol-5-yl)-2-(phenylamino)pyrimidine-5-carbonitrile CDK9 Inhibitors Suggest the Basis for Isoselectivity. *J. Med. Chem.* **2013**, *56*, 660–670.

(52) Lafleur, K.; Dong, J.; Huang, D.; Caflich, A.; Nevado, C. Optimization of inhibitors of the tyrosine kinase EphB4. 2. Cellular potency improvement and binding mode validation by X-ray crystallography. *J. Med. Chem.* **2013**, *56*, 84–96.

(53) Tshako, A. L.; Brown, D. S.; Koltun, E. S.; Aay, N.; Arcalas, A.; Chan, V.; Du, H.; Engst, S.; Franzini, M.; Galan, A.; Huang, P.; Johnston, S.; Kane, B.; Kim, M. H.; Laird, A. D.; Lin, R.; Mock, L.; Ngan, I.; Pack, M.; Stott, G.; Stout, T. J.; Yu, P.; Zaharia, C.; Zhang,

W.; Zhou, P.; Nuss, J. M.; Kearney, P. C.; Xu, W. The design, synthesis, and biological evaluation of PIM kinase inhibitors. *Bioorg. Med. Chem. Lett.* **2012**, *22*, 3732–3738.

(54) Staben, S. T.; Siu, M.; Goldsmith, R.; Olivero, A. G.; Do, S.; Burdick, D. J.; Heffron, T. P.; Dotson, J.; Sutherland, D. P.; Zhu, B. Y.; Tsui, V.; Le, H.; Lee, L.; Lesnick, J.; Lewis, C.; Murray, J. M.; Nonomiya, J.; Pang, J.; Prior, W. W.; Salphati, L.; Rouge, L.; Sampath, D.; Sideris, S.; Wiesmann, C.; Wu, P. Structure-based design of thienobenzoxepin inhibitors of PI3-kinase. *Bioorg. Med. Chem. Lett.* **2011**, *21*, 4054–4058.

(55) Fugel, W.; Oberholzer, A. E.; Gschloessl, B.; Dzikowski, R.; Pressburger, N.; Preu, L.; Pearl, L. H.; Baratte, B.; Ratin, M.; Okun, I.; Doerig, C.; Kruggel, S.; Lemcke, T.; Meijer, L.; Kunick, C. 3,6-Diamino-4-(2-halophenyl)-2-benzoylthieno[2,3-*b*]pyridine-5-carbonitriles are selective inhibitors of *Plasmodium falciparum* glycogen synthase kinase-3. *J. Med. Chem.* **2013**, *56*, 264–275.

(56) Bhattacharya, S. K.; Aspnes, G. E.; Bagley, S. W.; Boehm, M.; Brosius, A. D.; Buckbinder, L.; Chang, J. S.; Dibrino, J.; Eng, H.; Frederick, K. S.; Griffith, D. A.; Griffor, M. C.; Guimaraes, C. R.; Guzman-Perez, A.; Han, S.; Kalgutkar, A. S.; Klug-McLeod, J.; Garcia-Irizarry, C.; Li, J.; Lippa, B.; Price, D. A.; Southers, J. A.; Walker, D. P.; Wei, L.; Xiao, J.; Zawistoski, M. P.; Zhao, X. Identification of novel series of pyrazole and indole-urea based DFG-out PYK2 inhibitors. *Bioorg. Med. Chem. Lett.* **2012**, *22*, 7523–7529.

(57) Forsyth, T.; Kearney, P. C.; Kim, B. G.; Johnson, H. W.; Aay, N.; Arcalas, A.; Brown, D. S.; Chan, V.; Chen, J.; Du, H.; Epshteyn, S.; Galan, A. A.; Huynh, T. P.; Ibrahim, M. A.; Kane, B.; Koltun, E. S.; Mann, G.; Meyr, L. E.; Lee, M. S.; Lewis, G. L.; Noguchi, R. T.; Pack, M.; Ridgway, B. H.; Shi, X.; Takeuchi, C. S.; Zu, P.; Leahy, J. W.; Nuss, J. M.; Aoyama, R.; Engst, S.; Gendreau, S. B.; Kassees, R.; Li, J.; Lin, S. H.; Martini, J. F.; Stout, T.; Tong, P.; Woolfrey, J.; Zhang, W.; Yu, P. SAR and in vivo evaluation of 4-aryl-2-aminoalkylpyrimidines as potent and selective Janus kinase 2 (JAK2) inhibitors. *Bioorg. Med. Chem. Lett.* **2012**, *22*, 7653–7658.

(58) Wenglow, S.; Moreno, D.; Laird, E. R.; Gloor, S. L.; Ren, L.; Risom, T.; Rudolph, J.; Sturgis, H. L.; Voegtli, W. C. Pyrazolopyridine inhibitors of B-Raf(V600E). Part 4: rational design and kinase selectivity profile of cell potent type II inhibitors. *Bioorg. Med. Chem. Lett.* **2012**, *22*, 6237–6241.

(59) Zapf, C. W.; Gerstenberger, B. S.; Xing, L.; Limburg, D. C.; Anderson, D. R.; Caspers, N.; Han, S.; Aulabaugh, A.; Kurumbail, R.; Shukla, S.; Li, X.; Spaulding, V.; Czerwinski, R. M.; Seth, N.; Medley, Q. G. Covalent inhibitors of interleukin-2 inducible T cell kinase (itk) with nanomolar potency in a whole-blood assay. *J. Med. Chem.* **2012**, *55*, 10047–10063.

(60) Ranjitkar, P.; Perera, B. G.; Swaney, D. L.; Hari, S. B.; Larson, E. T.; Krishnamurthy, R.; Merritt, E. A.; Villen, J.; Maly, D. J. Affinity-based probes based on type II kinase inhibitors. *J. Am. Chem. Soc.* **2012**, *134*, 19017–19025.

(61) Aronov, A. M.; Baker, C.; Bemis, G. W.; Cao, J.; Chen, G.; Ford, P. J.; Germann, U. A.; Green, J.; Hale, M. R.; Jacobs, M.; Janetka, J. W.; Maltais, F.; Martinez-Botella, G.; Namchuk, M. N.; Straub, J.; Tang, Q.; Xie, X. Flipped out: structure-guided design of selective pyrazolopyrrole ERK inhibitors. *J. Med. Chem.* **2007**, *50*, 1280–1287.

(62) Williams, N. K.; Bamert, R. S.; Patel, O.; Wang, C.; Walden, P. M.; Wilks, A. F.; Fantino, E.; Rossjohn, J.; Lucet, I. S. Dissecting specificity in the Janus kinases: the structures of JAK-specific inhibitors complexed to the JAK1 and JAK2 protein tyrosine kinase domains. *J. Mol. Biol.* **2009**, *387*, 219–232.

(63) Huang, D.; Zhou, T.; Lafleur, K.; Nevado, C.; Caflich, A. Kinase selectivity potential for inhibitors targeting the ATP binding site: a network analysis. *Bioinformatics* **2010**, *26*, 198–204.

(64) Jeffrey, P. D.; Russo, A. A.; Polyak, K.; Gibbs, E.; Hurwitz, J.; Massague, J.; Pavletich, N. P. Mechanism of CDK activation revealed by the structure of a cyclinA-CDK2 complex. *Nature* **1995**, *376*, 313–320.

(65) Lin, W. H.; Song, J. S.; Chang, T. Y.; Chang, C. Y.; Fu, Y. N.; Yeh, C. L.; Wu, S. H.; Huang, Y. W.; Fang, M. Y.; Lien, T. W.; Hsieh, H. P.; Chao, Y. S.; Huang, S. F.; Tsai, S. F.; Wang, L. M.; Hsu, J. T.;

Chen, Y. R. A cell-based high-throughput screen for epidermal growth factor receptor pathway inhibitors. *Anal. Biochem.* **2008**, *377*, 89–94.

(66) Vagin, A.; Teplyakov, A. MOLREP: an automated program for molecular replacement. *J. Appl. Crystallogr.* **1997**, *30*, 1022–1025.

(67) Bailey, S. The CCP4 suite: programs for protein crystallography. *Acta Crystallogr., Sect. D: Biol. Crystallogr.* **1994**, *50*, 760–763.

(68) Murshudov, G. N.; Vagin, A. A.; Dodson, E. J. Refinement of macromolecular structures by the maximum-likelihood method. *Acta Crystallogr., Sect. D: Biol. Crystallogr.* **1997**, *53*, 240–255.

(69) Jones, T. A.; Zou, J. Y.; Cowan, S. W.; Kjeldgaard, M. Improved methods for building protein models in electron density maps and the location of errors in these models. *Acta Crystallogr., Sect. A: Found. Crystallogr.* **1991**, *47*, 110–119.

(70) Joosten, R. P.; Salzemann, J.; Bloch, V.; Stockinger, H.; Berglund, A.-C.; Blanchet, C.; Bongcam-Rudloff, E.; Combet, C.; Da Costa, A. L.; Deleage, G.; Diarena, M.; Fabbretti, R.; Fettahi, G.; Flegel, V.; Gisel, A.; Kasam, V.; Kervinen, T.; Korpelainen, E.; Mattila, K.; Pagni, M.; Reichstadt, M.; Breton, V.; Tickle, I. J.; Vriend, G. PDB_REDO: automated re-refinement of X-ray structure models in the PDB. *J. Appl. Crystallogr.* **2009**, *42*, 376–384.

(71) Chen, V. B.; Arendall, W. B., III; Headd, J. J.; Keedy, D. A.; Immormino, R. M.; Kapral, G. J.; Murray, L. W.; Richardson, J. S.; Richardson, D. C. MolProbity: all-atom structure validation for macromolecular crystallography. *Acta Crystallogr., Sect. D: Biol. Crystallogr.* **2010**, *66*, 12–21.